Aerogel-Based 3D Printed Optofluidic Waveguided Multi-Channel Photocatalytic Microreactors

by

Jhan Luke OKKABAZ

A Dissertation Submitted to the
Graduate School of Sciences and Engineering
in Partial Fulfillment of the Requirements for
the Degree of

Master of Science

in

Computer Science and Engineering

KOÇ ÜNİVERSİTESİ

September 18, 2024

Aerogel-Based 3D Printed Optofluidic Waveguided Multi-Channel Photocatalytic Microreactors

Koç University

Graduate School of Sciences and Engineering

This is to certify that I have examined this copy of a master's thesis by

Jhan Luke OKKABAZ

and have found that it is complete and satisfactory in all respects,

and that any and all revisions required by the final

examining committee have been made.

Committee Members:

____

Prof. Dr. Alper Kiraz

____

Prof. Dr. Can Erkey

____

Assist. Prof. Dr. Berna Morova

Date: ______________________________

I would like to dedicate this thesis to those who have supported and guided me throughout this journey.

First and foremost, to my beloved mother, sister, and father, whose unwavering support, love, and encouragement have been my strength. Your belief in me has kept me motivated, even through the most challenging moments. I am deeply grateful for all the sacrifices you've made and the trust you placed in me. Thank you for being there whenever I needed you and for always supporting every decision I made (even those decisions that, in hindsight, probably needed a little more thinking through).

To my supervisor, Prof. Dr. Alper Kiraz, I owe a tremendous debt of gratitude for providing this opportunity. Your guidance, insight, and patience have been invaluable throughout this process. You have given me not only the tools to navigate academia but also a great view of life in it. Your mentorship has shaped not only this work but also my growth as a researcher.

I would also like to thank the committee members for their time, feedback, and invaluable contributions to my work. Your insights have been crucial in shaping the direction and quality of this research.

Thank you for not disowning me despite my persistent nerdy inquiries and for always being there to help, laugh, and prove that life inside the lab can actually be fun too. You've shown me that a lab-life balance is not only possible but also full of unexpected laughs, coffee breaks, and moments that remind me why I chose this path in the first place.

To my lab members, whose collaboration and camaraderie have made this journey both productive and enjoyable, I am thankful for the countless discussions, experiments, and moments of mutual support.

Finally, to all my collaborators who contributed their expertise and time to this research, your partnership has been vital to the completion of this thesis.

ABSTRACT

Aerogel-Based 3D Printed Optofluidic Waveguided Multi-Channel Photocatalytic Microreactors

Jhan Luke OKKABAZ

Master of Science in Computer Science and Engineering

September 18, 2024

This thesis investigates the use of additive 3D printing technology for creating micro photoreactors within aerogels. The study focuses on developing a low-cost 3D printing system tailored for aerogels and optimizing an ink formulation suitable for 3D printing processes. The research begins with customizing an off-the-shelf 3D printer to fabricate a low-cost system specifically for aerogel-based structures. This customized printer integrates a 3D-printed syringe pump system and custom software for accurate calibration and printing of sub-millimeter lines. The ink formulation designed for 3D printing comprises a silica aerogel starter solution with additives and titanium dioxide nanoparticles. Post-printing steps including gelation and solvent exchange refine the aerogel's structures enhancing stability for micro photoreactors designed to interact with water. Rheological characterization studies inform ink optimization ensuring durability and usability over time. The optimized 3D printing system and ink formulations demonstrate advancements in printing aerogels with additives where applications promise impactful solutions and future advancements in materials engineering and environmental sciences.

ÖZETÇE

Aerogel Tabanlı 3D Baskılı Optofluidik Dalga Kılavuzlu Çok Kanallı Fotokatalitik Mikroreaktörler

Jhan Luke OKKABAZ

Bilgisayar Bilimleri ve Mühendisliği, Yüksek Lisans

18 Eylül 2024

Bu tez, aerogeller içinde mikro fotoreaktörler oluşturmak için eklemeli 3D baskı teknolojisinin kullanımını araştırmaktadır. Çalışma, aerogellere özel, düşük maliyetli bir 3D baskı sistemi geliştirmeyi ve 3D baskı süreçlerine uygun bir mürekkep formülasyonunu optimize etmeyi hedeflemektedir. Araştırma, piyasada bulunan bir 3D yazıcının, aerogel tabanlı yapılar için düşük maliyetli bir sistem oluşturmak amacıyla özelleştirilmesiyle başlar. Bu özelleştirilmiş yazıcı, 3D baskı şırınga pompası sistemi ve milimetre altı hatların doğru kalibrasyonu ve baskısı için özel bir yazılımı entegre eder. 3D baskıya uygun mürekkep formülasyonu, katkı maddeleri ve titanyum dioksit nanoparçacıkları içeren bir silika aerogel başlangıç çözeltisinden oluşur. Baskı sonrası yapılan jelleştirme ve çözücü değişim işlemleri, mikro fotoreaktörlerin su ile etkileşime geçmesi için aerogel yapılarının stabilitesini artırır. Reolojik karakterizasyon çalışmaları, mürekkep optimizasyonuna katkı sağlayarak dayanıklılık ve uzun vadeli kullanılabilirlik sağlar. Optimize edilen 3D baskı sistemi ve mürekkep formülasyonları, katkı maddeleriyle aerogellerin baskısında önemli ilerlemeler göstermekte olup, bu uygulamalar, malzeme mühendisliği ve çevre bilimlerinde gelecekteki yeniliklere ve etkili çözümlere zemin hazırlamaktadır.

AKNOWLEDGEMENTS

This work was supported by Tübitak 1001 project (grant no: 121M497).

A. Kiraz acknowledges partial support from the Turkish Academy of Sciences (TÜBA).

TABLE OF CONTENTS

LIST OF TABLES

LIST OF FIGURES

- **Figure 12:** Comparison of ink with air bubbles (before) and air-free ink (after). The improvement in print quality after air pocket removal is visualized here, with a side-by-side comparison.
- **Figure 13:** Printing on a metal grid surface. Initial tests on a metal grid showed inadequate adhesion, as seen in this figure.
- **Figure 14:** Printing on a glass slide surface, showing improvement in adhesion and quality. This figure demonstrates the successful use of glass slides as the substrate for printing.
- **Figure 15:** Printing on a glass slide surface, full-scale view. The microscope glass slide substrate allowed for practical post-processing, as seen in this image.
- **Figure 16:** Comparison of printing speeds at 13.5 mm/s and 40.5 mm/s. This figure illustrates the effect of different printing speeds on the final structure of the aerogel.
- **Figure 17:** Gelled grid structure after printing, showing internal wall thicknesses and grid cavities. The structural precision of the grid pattern is highlighted here, with measurements of wall and cavity sizes.
- **Figure 18:** TiO_2-based ink printed with manual G-code, showing grid gap sizes. This figure shows the fine control achieved using manual G-code, leading to precise grid designs with gap sizes as small as 0.05 mm.
- **Figure 19:** Viscosity of the silica-TiO_2 gel sample as a function of shear rate. Rheological data showing the shear-thinning behavior of the aerogel ink, which is critical for maintaining structure during printing.
- **Figure 20:** Storage modulus (G') and loss modulus (G'') for the silica-TiO_2 gel. This figure presents the gel's viscoelastic properties, confirming its suitability for 3D printing.
- **Figure 21:** Non-linear storage and viscous moduli of the ink sample. The rheological performance of the ink under strain is visualized here, providing insights into its mechanical behavior.
- **Figure 22:** Storage and viscous moduli recovery tests for the Silica-TiO_2 gel. This figure shows how the material recovers after deformation, indicating its resilience for long-term use.

- **Figure 23:** SEM images of TiO_2 particles within the aerogel structure at various scales. SEM analysis confirms the homogeneous dispersion of TiO_2 particles throughout the aerogel matrix.
- **Figure 24:** Stages from printing to the final dried aerogel product. This figure illustrates the full process from 3D printing to post-processing, including gelation and supercritical drying.
- **Figure 25:** Fully processed prints with varying TiO_2 percentages, showing differences in whiteness. The visual appearance of the aerogels, depending on the TiO_2 content, is shown in this image.
- **Figure 26:** Post-processed grid and cylindrical aerogel structures with sub-millimeter precision. This final figure highlights the structural integrity and precision of the aerogel after post-processing, demonstrating the effectiveness of the optimized printing method.
- **Figure 27:** The LED setup with a cylindrical tube silica aerogel microreactor sample mounted.
- **Figure 28:** UV-Vis spectrophotometric absorbance measurements at 270 nm were conducted on samples from Microreactor-2, collected at 5-minute intervals over a total duration of 160 minutes.

ABBREVIATIONS

SEM	Scanning Electron Microscopy
IPA	Isopropyl Alcohol
PLA	Polylactic Acid
ABS	Acrylonitrile Butadiene Styrene
SAOS	Small Amplitude Oscillatory Shear
LAOS	Large Amplitude Oscillatory Shear
HMDS	Hexamethyldisilane
DIW	Direct Ink Writing
G'	Storage Modulus
G''	Loss Modulus
FDM	Fused Deposition Modelling
PPGNH	Poly(propylene glycol) bis(2-aminopropyl ether)
LVR	Linear Viscoelastic Region

Chapter 1:
INTRODUCTION

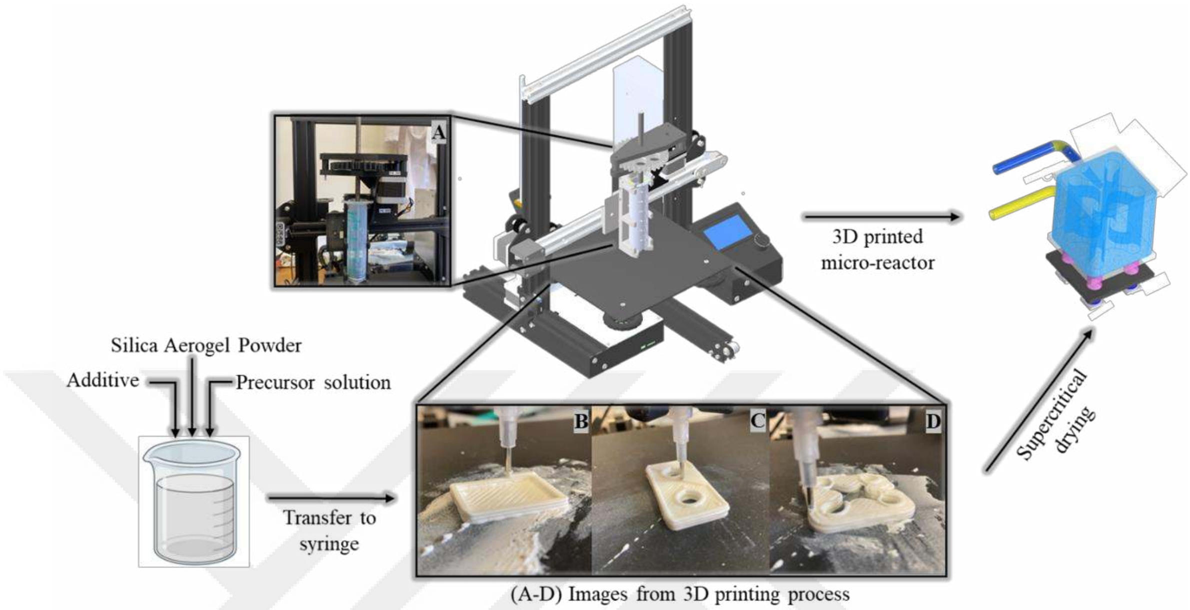

Fig. 1. Process from chemical production to microreactor.

1.1 Background

The advent of 3D printing, or additive manufacturing, has revolutionized numerous industries, enabling the creation of complex geometries and custom structures that were previously unattainable with conventional manufacturing methods. Since its inception in the 1980s, 3D printing has evolved significantly, expanding its reach from rapid prototyping to end-use production across various sectors, including aerospace, healthcare, automotive, and consumer goods [1][2][3]. The flexibility of 3D printing lies in its ability to fabricate objects layer by layer using diverse materials such as metals, polymers, ceramics, and biomaterials.

Aerogels, a class of highly porous and lightweight materials, have garnered significant attention due to their exceptional physical properties. These include extremely low thermal conductivity, low density, high surface area, and unique optical properties. Aerogels have been explored extensively for applications in thermal insulation, catalysis, energy storage, environmental remediation, and even in aerospace engineering [1]. The synthesis of aerogels typically involves sol-gel processes followed by supercritical drying to prevent pore collapse, which results in a highly porous solid network [4][5].

The convergence of 3D printing technology with aerogel production presents a groundbreaking opportunity to fabricate aerogels with tailored geometries and enhanced properties. Traditional methods of aerogel fabrication, while effective, often result in brittle structures with limited customization in shape and size. 3D printing offers a novel approach to overcome these limitations, enabling the precise deposition of aerogel-forming materials to create complex, multi-functional structures [6][7][3][8][5][9][10].

Recent advancements in direct ink writing (DIW) and other extrusion-based techniques have facilitated the 3D printing of aerogels, particularly silica-based and composite aerogels. These developments have been driven by the need for more efficient, scalable, and environmentally friendly manufacturing processes. The incorporation of additives such as titanium dioxide (TiO_2) has further expanded the functional capabilities of 3D-printed aerogels, particularly in applications like photocatalysis for environmental remediation [1][6][7][11][12][13][14].

1.2 Motivation

The primary motivation for this research stems from the growing demand for customized aerogel structures in various high-performance applications. Conventional aerogel manufacturing methods are limited in their ability to produce structures with intricate geometries or to integrate multiple functionalities within a single material. By leveraging 3D printing, it becomes possible to address these limitations, enabling the creation of aerogels with complex architectures and enhanced properties.

Current fabrication techniques for aerogels often involve labor-intensive processes that are not easily scalable. Furthermore, these methods are typically constrained by the material properties of aerogels, particularly their brittleness and tendency to shrink during drying [15]. The integration of 3D printing with aerogel production offers a potential solution to these challenges by providing greater control over the material deposition process, thereby reducing defects and improving the mechanical stability of the final product.

The development of 3D-printed aerogels also holds significant implications for environmental sustainability. Aerogels are known for their effectiveness in insulating and catalyzing chemical reactions, which can lead to energy savings and the reduction of harmful emissions. Moreover, the ability to 3D print aerogels using sustainable and recyclable materials aligns with global efforts to reduce the environmental impact of manufacturing processes [11].

1.3 Objectives

One of the primary objectives of this research is to develop a customized 3D printing system capable of fabricating high-resolution aerogel structures. This involves the modification of existing 3D printing hardware, such as the Creality Ender 3 Pro, to accommodate the unique rheological properties of aerogel inks. The development of a custom syringe pump system, designed to precisely control the extrusion of aerogel inks, is central to achieving this objective.

A critical aspect of this research is the formulation of aerogel inks that are compatible with the 3D printing process. This involves the synthesis of silica-based and composite aerogels, incorporating additives such as TiO_2 to enhance their functional properties. The rheological behavior of these inks, including their shear-thinning and viscoelastic properties, will be characterized and optimized to ensure successful printing [16][4].

The research also aims to thoroughly characterize the properties of the 3D-printed aerogel structures, including their surface area, and pore structure. Techniques such as scanning electron microscopy (SEM), nitrogen adsorption, and rheometry will be employed to assess the performance of the printed aerogels and to compare them with conventionally fabricated aerogels [17][4].

Finally, the research seeks to explore the potential applications of 3D-printed aerogels, particularly in the development of optofluidic waveguided multi-channel photocatalytic microreactors. These microreactors are designed to enhance the efficiency of photocatalytic reactions, which are critical for processes such as water purification and air filtration [7][16].

1.4 Literature Review

A review of the literature on aerogels reveals their development since the 1930s, when Samuel Stephens Kistler first introduced the concept of replacing the liquid component of a gel with a gas without causing shrinkage. Over the decades, significant advancements have been made in the synthesis and application of aerogels, particularly silica aerogels, which remain the most widely studied [15][5].

The literature on 3D printing technologies highlights the rapid evolution of this field, particularly in the context of material science. Key developments include the refinement of direct ink writing techniques and the customization of 3D printing hardware to handle a wider range of materials, including viscous inks and gels [18].

Recent studies have begun to explore the intersection of 3D printing and aerogel fabrication, with a focus on overcoming the material limitations associated with traditional aerogel manufacturing methods. Researchers have demonstrated the feasibility of using 3D printing to create aerogels with enhanced mechanical properties and custom geometries, although challenges such as ink formulation and print resolution remain [3][2][19].

The literature also emphasizes the functionalization of aerogels through the incorporation of various additives, such as metal oxides, to tailor their properties for specific applications. For example, the inclusion of TiO_2 in silica aerogels has been shown to significantly enhance their photocatalytic activity, making them suitable for environmental remediation applications [20] [17].

1.5 *Methodology*

The methodology involves the design and fabrication of a custom 3D printing system, starting with the selection of a suitable base printer (e.g., Creality Ender 3 Pro) and the development of a modular syringe pump system. This system will be engineered to handle the unique rheological properties of aerogel inks, with precise control over extrusion parameters.

The aerogel inks will be formulated using silica starter solution and TiO_2 as an additive, to achieve the desired rheological properties. The optimization process will involve adjusting the ink composition and testing its performance through rheological measurements, including viscosity, shear-thinning behavior, and viscoelasticity [4][16].

The optimized inks will be used to print aerogel structures, which will then undergo post-processing steps such as gelation, solvent exchange, and supercritical drying. The goal is to produce aerogels with minimal shrinkage and enhanced mechanical stability, suitable for various applications [7][2][21].

The printed aerogels will be characterized using a range of techniques, including SEM for morphological analysis, nitrogen adsorption for surface area measurement, and rheometry for mechanical property assessment. These characterizations will provide insights into the performance of the 3D-printed aerogels compared to traditional aerogels [17][20].

1.6 *Structure of the Thesis*

This thesis is organized into five chapters:

- **Chapter 1: Introduction** - Provides the background, motivation, objectives, and methodology of the research.
- **Chapter 2: 3D Printer** - Describes the 3D printer modifications and the custom syringe pump system used for printing the aerogel structures.
- **Chapter 3: Chemistry** - Discusses the formulation of the aerogel ink and the post-printing treatments applied to preserve the aerogel's properties.

- **Chapter 4: Results and Discussion** - Presents the findings of the research, including rheological properties, printing parameters and structural integrity.
- **Chapter 5: Conclusions** - Summarizes the key findings, discusses the implications and applications, and suggests directions for future work.

Chapter 2:
3D PRINTER

2.1 Introduction to 3D Printing in Aerogel Fabrication

The integration of 3D printing technology into the fabrication of aerogels represents a significant advancement in materials science and engineering. Traditional methods of aerogel production, although effective, often result in brittle structures with limited customization in geometry. The adoption of 3D printing offers an innovative approach to address these limitations, enabling the creation of aerogels with complex shapes and enhanced mechanical properties. This chapter discusses the development and optimization of a custom 3D printing system specifically designed for aerogel fabrication, detailing the hardware modifications, software enhancements, and the challenges encountered during the process.

2.2 Hardware Modifications for Aerogel 3D Printing

2.2.1 Selection of Base Printer

The Creality Ender 3 Pro 3D printer was selected as the base platform for this research due to its modular design, affordability, and widespread use within the 3D printing community. The printer's open-source architecture made it an ideal candidate for modification, allowing for the integration of custom components tailored to the specific requirements of aerogel ink extrusion. The selection was further influenced by the availability of replacement parts and the ease with which the printer could be adapted to handle the unique rheological properties of aerogel inks.

2.2.2 Development of a Custom Syringe Pump System

The modification of the 3D printer focused on replacing the traditional extruder system, typically used for thermoplastic filaments, with a custom syringe pump designed to handle the viscous, non-Newtonian aerogel inks used in this study. The standard fused deposition modeling (FDM) components, such as the extruder, heating element, and nozzle, were incompatible with the aerogel ink, necessitating this change. The custom syringe pump, driven by a NEMA 17 stepper motor and a T8 lead screw system, allowed for precise control over the extrusion process. By converting rotational motion into linear movement, the pump accurately pushed the syringe plunger to deposit the aerogel material layer by layer onto the print bed.

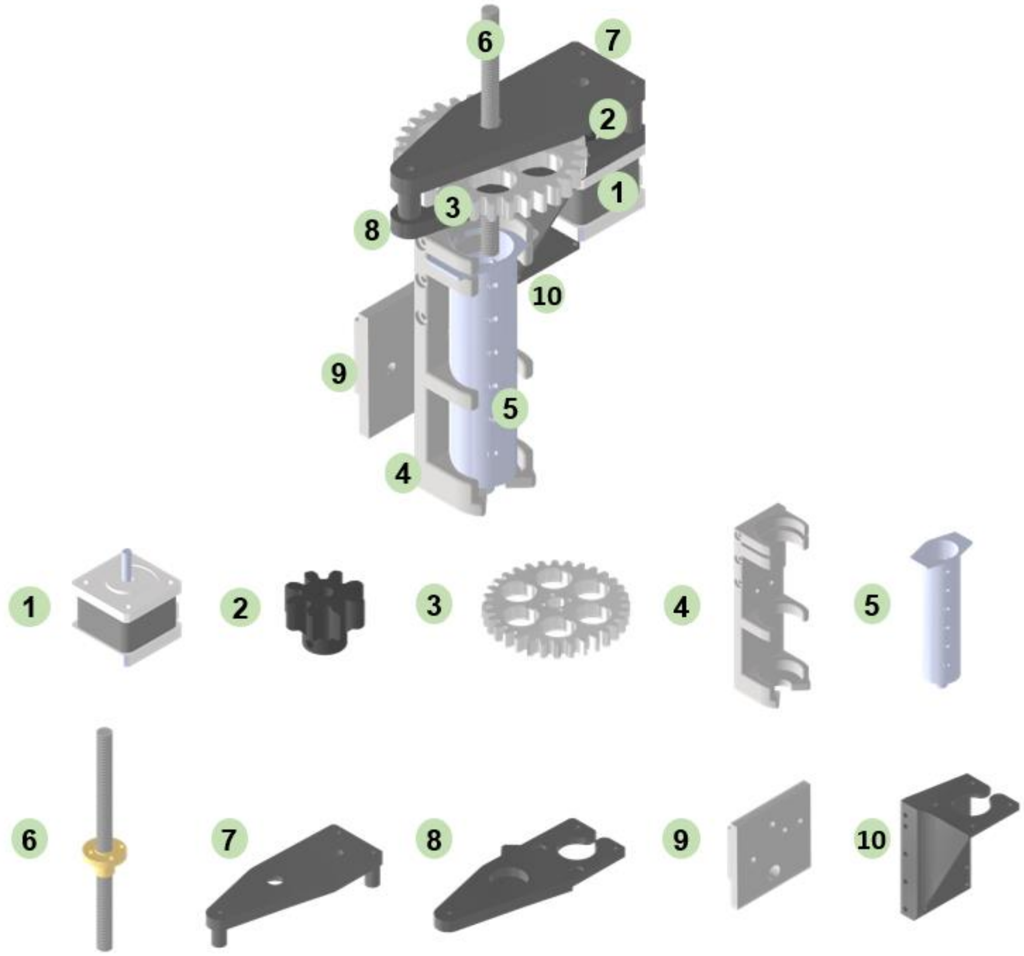

Fig. 2. Syringe pump parts. 1) Stepper motor. 2) Driving cog. 3) Driven cog. 4) Syringe holder. 5) Syringe. 6) T8 Lead Screw. 7) Upper cog holder. 8) Lower cog holder. 9) Backplate. 10) Motor mount. Parts 2,3,4,7,8,9 & 10 were 3D printed with an Ultimaker 2+.

The syringe pump system was designed with modularity in mind, facilitating easy disassembly for maintenance and experimentation with different aerogel formulations and additives. It could accommodate syringes ranging from 10 mL to 50 mL, providing flexibility in the volume of ink used for each print. Ball bearings were incorporated into the design to reduce friction, ensuring smooth and precise operation.

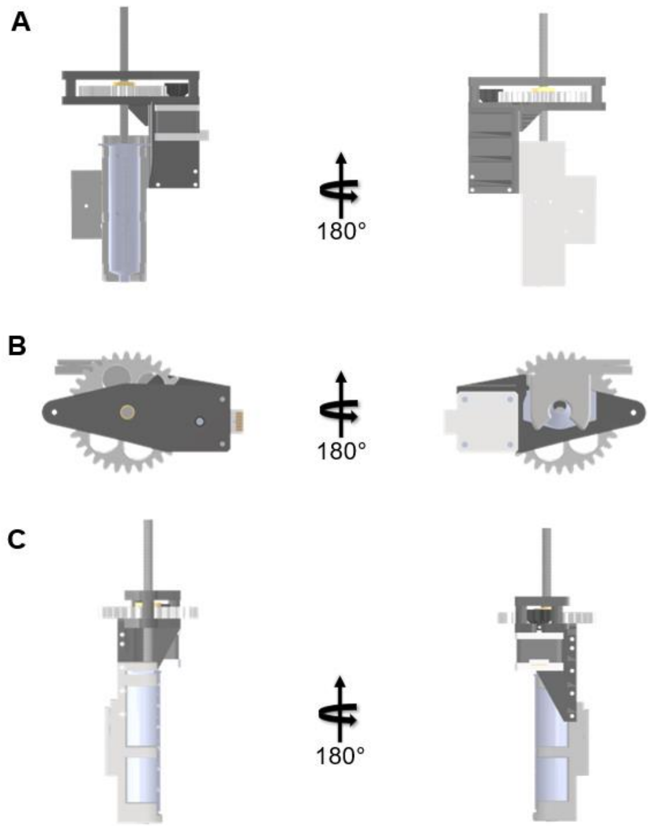

Fig. 3. Assembled syringe pump. A) Front, B) Top & Bottom, C) Side view.

A key challenge in 3D printing viscous materials like aerogel ink is the formation of air pockets, which can lead to extrusion inconsistencies and defects in the printed structure. To mitigate this, a series of steps were developed to remove air pockets, including tapping the syringe to release large bubbles and using a secondary syringe to eliminate smaller ones. This careful attention to detail ensured consistent and high-resolution printing results, overcoming the limitations of traditional FDM methods and adapting the printer to the unique properties of aerogel inks.

For The gear ratio between the driver and driven cogs is crucial for adjusting the analogue printing speed and torque. The relationship is given by (1):

$$Gear\ Ratio = \frac{n_1}{n_2} = \frac{T_2}{T_1} = \frac{d_2}{d_1} = \frac{Output\ torque}{Input\ torque} \tag{1}$$

where n represents gear speed, d is the diameter, and T is the number of teeth while subscript 1 is the driving cog and 2 is the driven cog. A higher gear ratio results in smaller step movements and higher torque but lower printing speeds, while a lower gear ratio allows for higher printing speeds but lower torque. This ratio can be adjusted to accommodate different syringe sizes, ink viscosities, and print designs. It is essential to ensure that the stepper motor has sufficient power to generate the required force. This formula can help for futures adjustment if more torque is needed.

2.3 Software Enhancements

2.3.1 Calibration and Control Software

The calibration and control of the syringe pump system were managed through custom software developed specifically for this research. The software, written in Python, allowed for real-time adjustments to the printer's operating parameters, including the extrusion rate, motor speed, and step size. This level of control was crucial for maintaining the consistency and accuracy of the printed aerogel structures. The software also included features such as manual G-code execution, linear movement control, and calibration terminals, providing the user with a comprehensive toolset for fine-tuning the printing process.

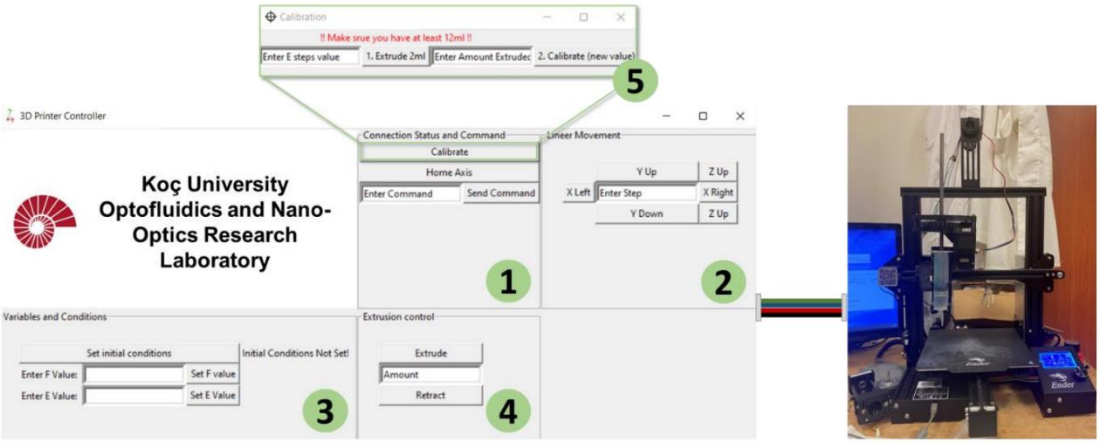

Fig. 4. Manual calibration software. 1) Manual G-code terminal and calibration. 2) Linear movement control. 3) Motor step and speed control 4) Extrude and retract terminal. 5) Calibration terminal.

The calibration process begins by setting an initial step value and filling the syringe with water. The water is extruded and weighed, and the weight is entered into the software to calculate a new step value. This process is repeated until the step value converges. This final step value is then used to modify the initial G-code so that the expected extrusion length matches the actual volume of extruded ink. Additionally, the software supports features such as cold extrusion, fan speed control, and print and bed temperature adjustments.

2.3.2 G-code Customization

G-code, the language used to control 3D printers, typically assumes the use of filament-based materials. To adapt this language for use with aerogel inks, several modifications were necessary. The custom software automatically generated G-code commands tailored to the specific needs of the syringe pump system. This included adjustments to the stepper motor's movement speed and direction, as well as modifications to the extrusion parameters to account for the non-Newtonian behavior of the aerogel inks. The software also supported the creation of complex geometries by allowing for the manual input of mathematical formulas, which were used to generate precise patterns and structures. Table 1 shows examples of G-Code codes and their functions.

Table 1. G-Code examples and their functions.

G-Code	Function	Description
G00	Rapid Positioning	Moves the syringe to a new position at high speed without extruding material.
G01	Linear Movement with Controlled Flow	Moves the syringe with controlled extrusion, accounting for flow rate changes.
G21	Set Units to Millimeters	Configures the system to interpret dimensions in millimeters.
G92	Set Current Position	Sets a reference position for the syringe and resets the coordinates to zero.
M106	Start Extrusion	Activates the syringe pump for controlled material extrusion.

The FullControl GCODE Designer software was employed for generating the G-codes required for the printing process. This software provided various base geometrical shapes which allowed for flexible design options tailored to the specific geometries needed. To keep track of the various designs, each file was saved in Excel sheets, organized by creation date.

Cold extrusion was enabled by adding a specific G-code command to the start sequence, making it possible to print without requiring heat. The Z-offset was fine-tuned based on the height of the syringe needle tips to ensure precise material application. Furthermore, adjustments were made to key parameters like bed temperature, filament diameter, and extrusion units, adapting them to the requirements of the syringe-pump system. The travel speed was initially set higher to simplify early testing and streamline the process.

The print speed varied depending on the structure of the microreactors and the needle size. The layer height parameter was adjusted as needed to accommodate the different syringe tips used in the process. Repetier-Host software was used to communicate these custom printing commands to the 3D printer.

Chapter 3:
CHEMISTRY

3.1 Introduction

The chemistry underlying the development and optimization of aerogel-based 3D printed optofluidic waveguided multi-channel photocatalytic microreactors is a critical aspect of this research. This chapter delves into the chemical principles and processes involved in the formulation of aerogel inks, the incorporation of photocatalytic materials, and the post-printing treatments that ensure the stability and functionality of the aerogel structures. By integrating advanced materials chemistry with additive manufacturing techniques, this research aims to create innovative solutions for environmental remediation and other applications.

The core of this work involves the use of silica aerogels, known for their exceptional properties such as high porosity, low density, and large surface area. These properties make them ideal candidates for photocatalytic applications, especially when combined with TiO_2 nanoparticles, which are well-known for their photocatalytic efficiency. The successful integration of these materials into a 3D printable ink and the subsequent fabrication of stable and functional aerogel structures require a thorough understanding of their chemistry and interactions.

Recent advancements in aerogel chemistry and 3D printing technology have opened new avenues for creating multifunctional materials with tailored properties. The recent studies on the additive manufacturing of silica aerogels demonstrates the potential of these materials for creating lightweight and thermally insulating structures [10]. Similarly, studies have explored the use of 3D printing for microelectronic packaging, highlighting the versatility of this technology [22]. The incorporation of photocatalytic components into aerogels further enhances their functionality, which have been demonstrated studies by their development of aerogel-based photocatalytic microreactors [13] [16].

3.2 *Aerogel Ink Formulation*

Formulating a suitable ink is a critical step in the development of 3D-printed aerogel structures. By building on previously developed formulations [16][13], we enhanced the base composition by incorporating specific additives to tailor the aerogel's properties for targeted applications, such as photocatalytic environmental remediation. TiO_2 was selected as the key additive because of its well-established photocatalytic properties, which are essential for applications like pollutant breakdown and improving photocatalytic efficiency [16][23]. The integration of TiO_2 into the aerogel matrix was intended to optimize the material for multifunctional use in environmental applications [20].

The formulation of the aerogel ink began with the preparation of a base solution that included Dynasylan 40 (a silica solution containing 40-42 wt.% SiO_2), 1-pentanol, and nitric acid (HNO_3), sourced from Evonik Industries and Sigma-Aldrich. Initially, 2 ml of Dynasylan 40, 2.2 ml of 1-pentanol, and 0.16 ml of distilled water were combined and stirred at 35°C for 10 minutes at a rate of 250 rpm. The solution was allowed to cool to room temperature before the addition of 5.2 µl of HNO_3, followed by an additional 5 minutes of stirring. The mixture was then stored at 4°C for 24 hours to ensure adequate hydrolysis and condensation of the silica starter solution. The composition of the ink is summarized in Table 2.

Table 2. Silica aerogel ink composition. *After hydrolysis.

Dynasylan -40 (ml)	1-Pentanol (ml)	HNO_3 (µl)	Water (ml)	Aerogel Particles (g)	PPGNH (ml)	1-Pentanol* (ml)	TiO_2 (g)	HCl (µl)
2	2.2	5.2	0.16	0.86	0.73	9	0.7	0.1

After 24 hours, the solution was brought back to room temperature, and a secondary mixture was prepared by combining 9 ml of 1-pentanol with 0.73 ml of poly(propylene glycol) bis(2-aminopropyl ether) (PPGNH) and stirring at 500 rpm for 5 minutes. The addition of PPGNH served to increase viscosity and promote a homogeneous ink mixture, minimizing the potential for clumping of the silica aerogel particles. Next, 0.1 µl of hydrochloric acid (HCl, 37%) was added, followed by another 5 minutes of stirring. To this mixture, 0.86 g of silica aerogel particles (5–20 µm) and 0.7 g of TiO_2 nanoparticles were introduced. These amounts, corresponding to 100 wt.% and 50 wt.% relative to the SiO_2 content, were carefully balanced to optimize the relationship between the aerogel matrix and the functional additive. Finally, the mixture was stirred at 1500 rpm using a propeller to ensure complete dispersion and homogeneity.

3.3 *Post-Printing Gelation and Solvent Exchange*

Once the aerogel ink is extruded through the 3D printing system, it must undergo a controlled gelation process to transition from a soft, extruded state to a rigid, self-supporting structure. Without this transformation, the printed aerogel structure would collapse during subsequent drying. Gelation was initiated by placing the printed structures in an airtight chamber containing 1.7 ml of ammonia solution. The exposure time was adjusted according to the thickness of the printed structures, ranging from 20 minutes for thin layers to 180 minutes for thicker constructs.

Following gelation, the aerogels underwent a solvent exchange process to replace the original solvents (primarily 1-pentanol) with ethanol. The printed gels were submerged in a solution of 95% ethanol and 5% 2-propanol for 24 hours to begin this process. After the initial immersion, the solution was replaced with 100% ethanol, and the exchange was repeated until all 1-pentanol was removed from the gel. This step is critical for preparing the aerogel structures for supercritical drying, which preserves the porous network and prevents shrinkage.

3.4 *Supercritical Drying and Final Structure*

To avoid structural collapse during drying, the gelled aerogels were dried using supercritical CO_2. The gel was placed in a high-pressure vessel filled with ethanol, and the Applied Separations Speed SFE unit was used to conduct supercritical drying at 85 bar and 50°C for 4 hours. During this process, the ethanol was exchanged with supercritical CO_2, which was gradually vented, allowing the aerogel to dry without pore collapse. Paper meshes (similar to tea bags) were used to hold the gel during drying, ensuring that the fragile structures remained intact.

The final product was a 3D-printed silica-TiO_2 aerogel structure with uniform porosity and enhanced photocatalytic properties, as shown in Figure 5. In applications requiring hydrophobic surfaces, additional surface treatments such as hexamethyldisilane (HMDS) exposure could be employed to modify the surface chemistry, further expanding the material's applicability in diverse environmental conditions [24].

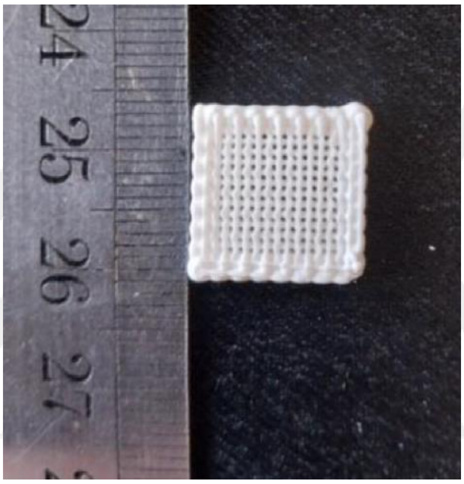

Fig. 5. 3D printed grid aerogel structure with TiO_2 as an additive.

Chapter 4:
RESULTS AND DISCUSSION

4.1 Ink Formulation and Rheological Testing

During the testing phase, five different aerogel ink compositions were evaluated to determine the optimal formulation. The ink formulation process involved three key components: (1) a starter solution, (2) a mixture of PPGNH, HCl, and 1-pentanol, and (3) silica aerogel and TiO_2, which directly impacted the target properties. The first two components were kept constant while varying the ratio of silica aerogel and TiO_2 in the third component, as shown in Figure 6.

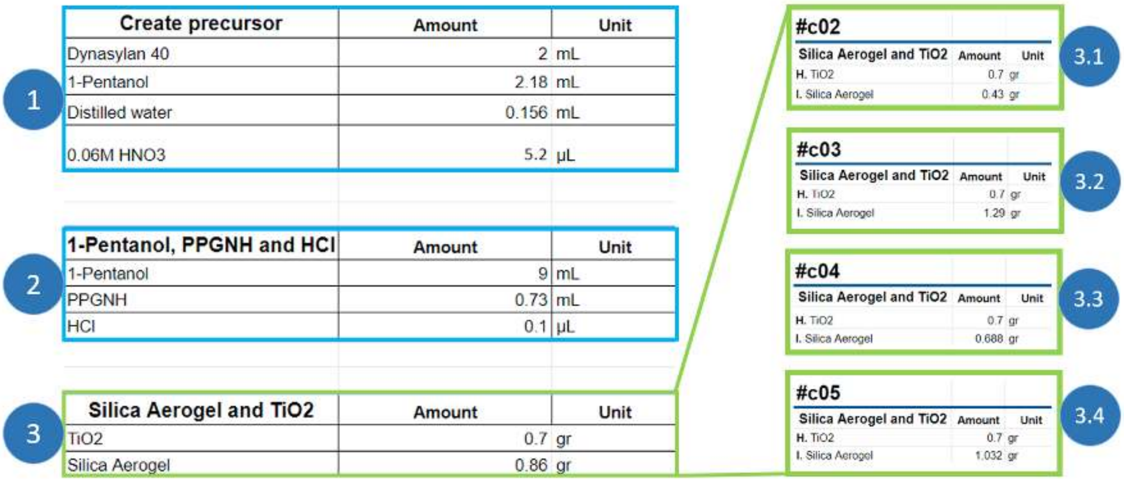

Fig. 6. The base formulation. 1) Starter solution. 2) Second step mixture. 3) Silica aerogel formulations with different ratios of silica powder.

It was found that increasing the TiO_2 content significantly impacted the printing resolution due to clogging, particularly when the TiO_2 content exceeded 300-600% of the base formulation. In contrast, the silica aerogel ratio had a direct effect on the viscosity of the ink. When the silica aerogel content was reduced by 50%, the viscosity decreased non-linearly, leading to structures that could not support themselves. Conversely, increasing the silica content by 50% resulted in excessively high viscosity, which compacted the ink during printing and eliminated its shear-thinning properties.

Through these tests, it was determined that maintaining the silica aerogel content within ±20% of the base formulation provided the best balance for printability. This finding highlighted the need for precise optimization of the silica aerogel content based on the other components of the ink to ensure successful printing. The recommended formulation allows for reliable printing with consistent structural integrity.

4.2 Pre-Print Setup

Prior to printing, the printer underwent calibration and bed leveling, with a glass slide positioned as the substrate for the aerogel structure. Careful preparation was critical to minimize potential failures during post-processing, ensuring all steps were ready. After preparing the aerogel ink, it was promptly loaded into syringes within 10 minutes to prevent solvent evaporation and maintain its rheological properties, which will be discussed in detail in the following section.

A significant challenge encountered during the 3D printing process was the formation of macro- and micro-scale air pockets within the syringes during the ink loading process. These air pockets caused inconsistent extrusion and blockages, leading to variability in print quality. As shown in Figure 7, an air pocket removal process was essential to improve print consistency.

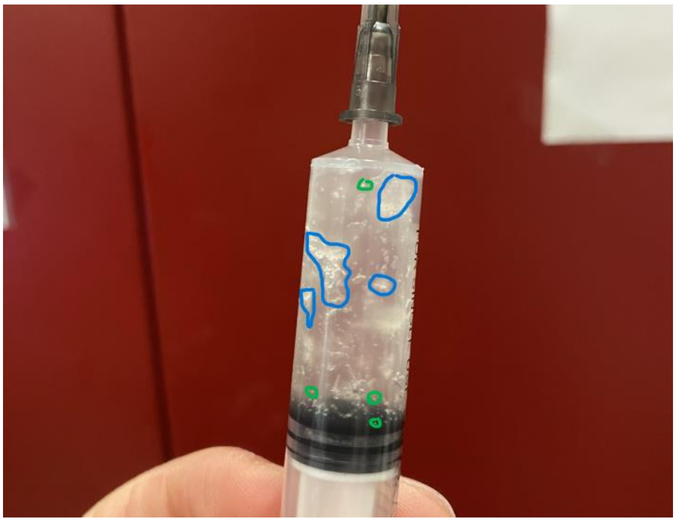

Fig. 7. Syringe filled with TiO_2-free ink. Blue: Macro air bubbles. Green: Micro air bubbles.

The syringe was inverted and gently tapped to allow larger air pockets to rise to the surface, which were then removed using standard syringe techniques. For smaller air pockets, an additional syringe was connected via silicone tubing, allowing air to escape through a small puncture while ensuring the ink did not leak. This method ensured the ink mixture was homogeneous and suitable for consistent printing. These steps were critical to achieving high-quality 3D prints, enhancing both the structural integrity and precision of the aerogel structures.

As shown in Figure 8, a test was conducted using a TiO_2-free ink to visualize the formation of air pockets more clearly as the addition TiO_2 make the in opaque. The image revealed that both macro and micro air pockets formed inside the syringe. These air bubbles caused inconsistencies during printing, leading to issues such as nozzle blockages and sudden bursts of ink, as illustrated in Figures 9 and 10.

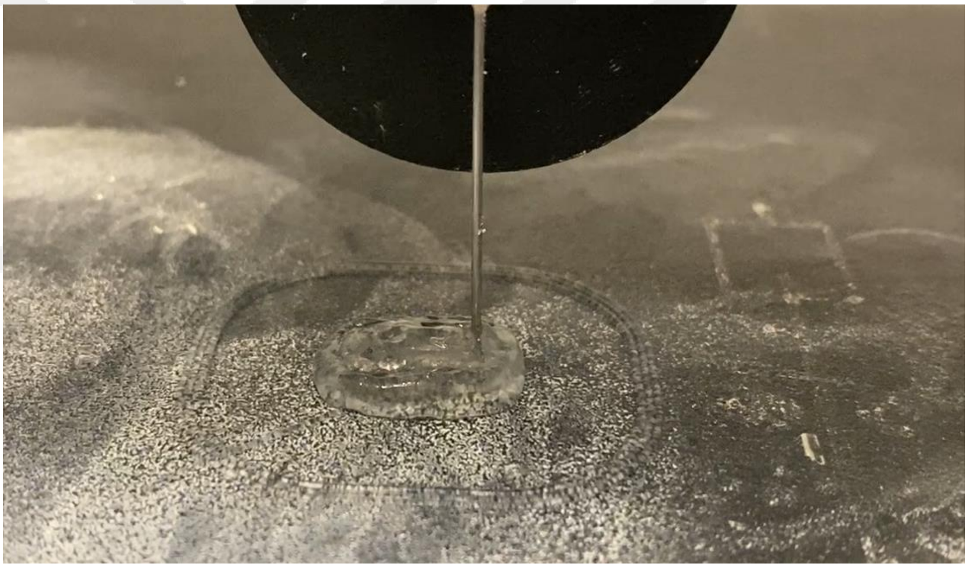

Fig. 9. TiO_2-free ink with air bubbles during printing.

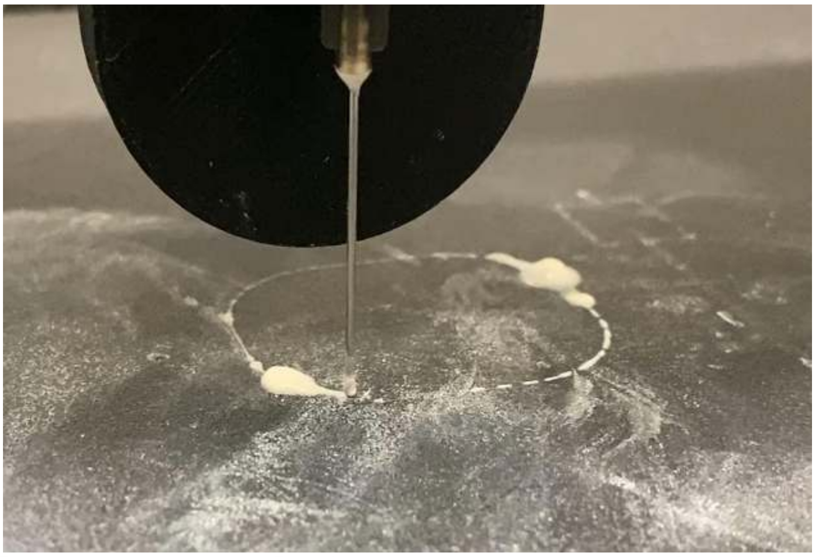

Fig 10. TiO_2 added ink with air bubbles during printing.

To address these issues, the syringe was gently tapped to remove the larger bubbles, followed using silicone tubing connected to an empty syringe, as shown in Figure 11. A fine needle was used to create a small puncture in the tubing, allowing the air to escape while transferring the ink to the empty syringe. This process removed 99% of the air bubbles, ensuring the ink was free of inconsistencies for printing.

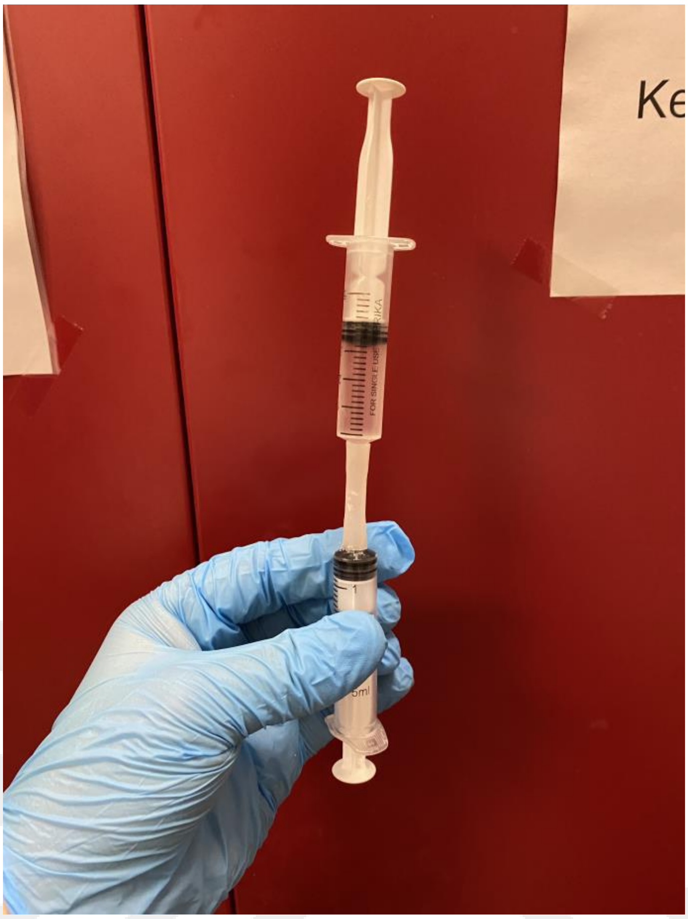

Fig. 11. Air bubble removal setup with silicone tubing.

Once the air pocket removal was complete, the ink was ready for printing, as seen in Figure 12. The irregular lines caused by air pockets, as observed in Figures 9 and 10, were no longer present after this process.

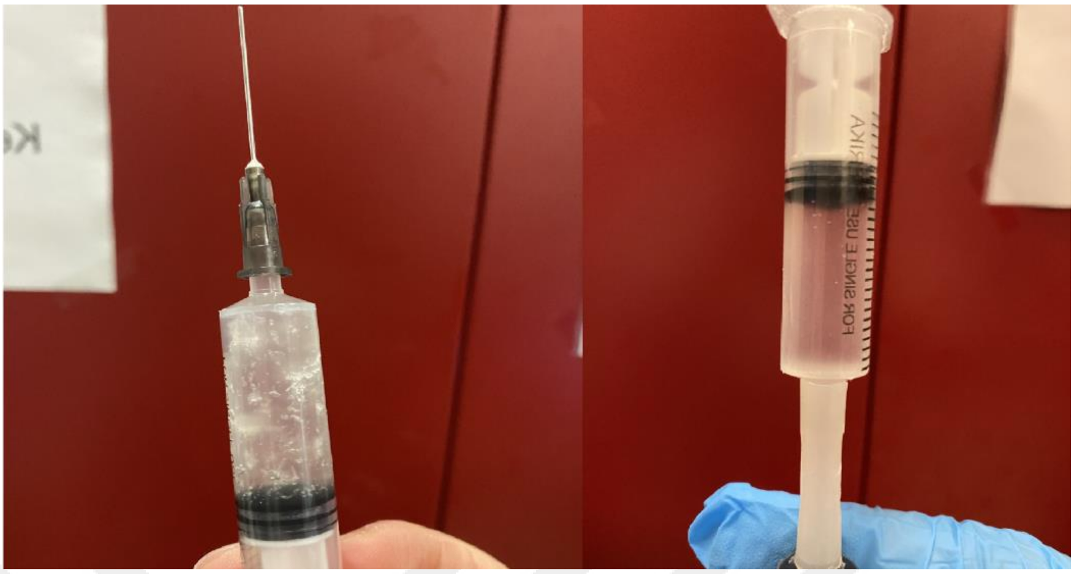

Fig. 12. Left) Ink with macro and micro air bubbles. Right) Ink after air bubble removal.

With the air-free ink-filled syringes prepared, the glass slides were securely positioned, and the desired nozzle size was attached. The syringe was then mounted onto the pump, marking the initiation of the printing process. One additional challenge encountered during this phase was the wear of the motor gear due to friction and heat generation. This was mitigated by printing small replacement gears using the Ultimaker 2+, which effectively resolved the issue and enabled continuous aerogel printing without mechanical disruptions.

Initial printing tests were conducted using the magnetic bed included with the Ender 3 Pro V2. While the bed provided sufficient adhesion, it was impractical for subsequent gelation and drying steps, as uniform exposure to the environment is essential for these processes. A metal grid surface was also tested to address this issue. However, as shown in Figure 13, the first layer did not adhere properly to the grid, causing the print to fail.

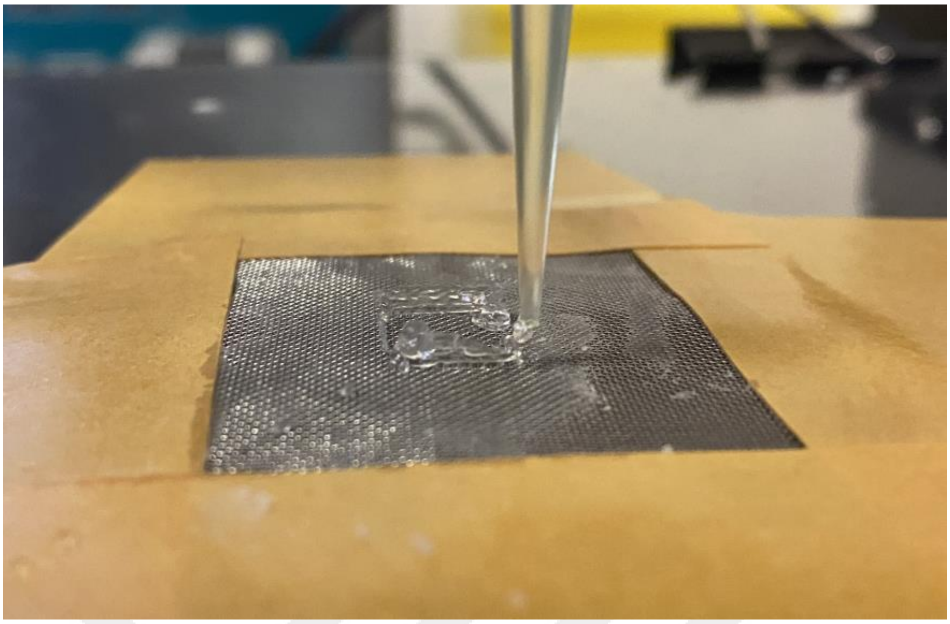

Fig. 13. Printing on a metal grid surface.

Glass slides were then tested as a surface for printing, and they quickly proved to be an ideal choice. The smoothness and uniformity of the glass offered excellent adhesion during the printing process, ensuring consistent layer deposition and high-quality prints. This addressed the adhesion issues seen with the metal grid surface, as shown in Figure 14, where the first layer struggled to stick, leading to print failures. As a result, glass slides were selected as the default substrate for subsequent prints.

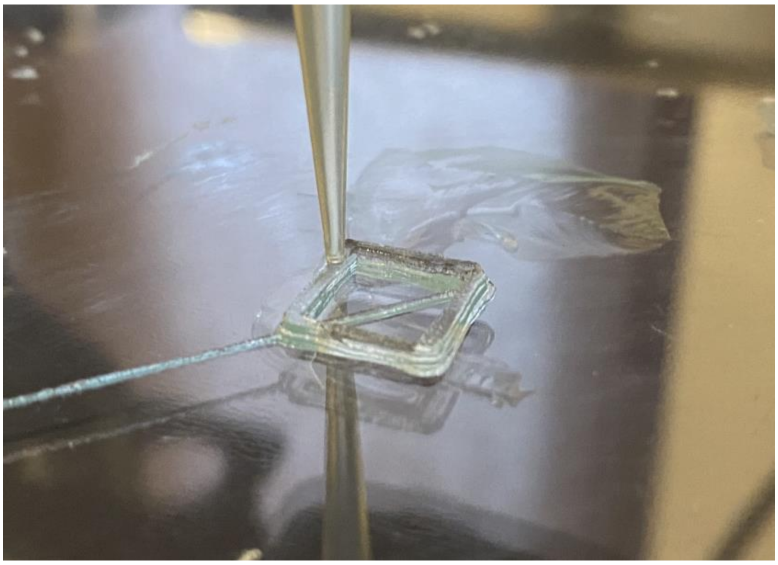

Fig. 14. Printing on a glass slide surface.

In addition to their printing benefits, glass slides also provided practical advantages during the post-processing stages. The 75mm x 24.75mm x 1mm microscope slides, as shown in Figure 15, allowed for effective gelation and drying processes. Their size and non-porous surface ensured that the printed aerogel structures were evenly exposed to the environment, making them ideal for multiple rounds of gelation and solvent exchange without the need for transferring or repositioning the printed objects.

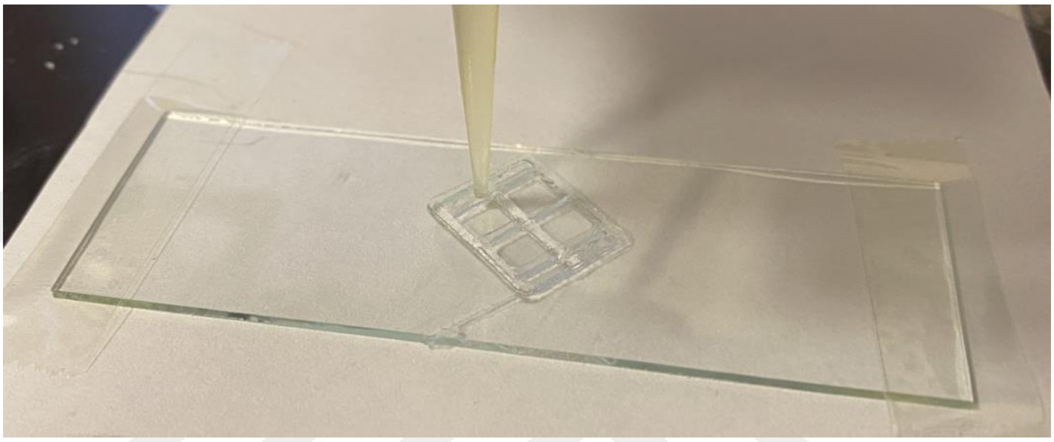

Fig. 15. Printing on a glass slide surface, full scale view.

Despite resolving surface-related issues, nozzle size remained a limiting factor. For nozzle diameters smaller than 0.05 mm, the syringe pump and stepper motor lacked the force required to extrude the ink effectively. As a result, printing with smaller nozzles was not feasible. For 0.1 mm nozzles, exploring different nozzle types, motors, ink compositions, and environmental conditions are needed to optimize the balance between precision and printability.

These optimizations in both surface selection and nozzle configuration significantly improved the reliability and quality of the 3D printing process, allowing to produce consistent aerogel structures with minimal defects. Continued refinement of these parameters is expected to enhance the overall precision and performance of aerogel printing.

4.3 *Printing Optimization and Design*

Print speed is directly related to the ink's rheological properties. Newtonian fluids with low viscosity cannot form stable structures, while highly viscous Newtonian fluids lead to excessive pressure within the syringe, making extrusion difficult. The aerogel ink used in this process is non-Newtonian and shear-thinning. The relationship between its storage modulus (G') and loss modulus (G") determines the optimal printing speed. The region where G" > G' defines the nonlinear viscoelastic region, which begins when sufficient stress is applied, allowing the ink to flow and exhibit liquid-like behavior. As long as the ink satisfies the shear-thinning criteria at a given speed and syringe size, printing can proceed effectively.

Testing was conducted using an 11.5 mm inner diameter syringe and a 0.4 mm nozzle, with printing speeds ranging between 13.5 mm/s and 40.5 mm/s, as shown in Figure 16**.** Syringe flow rates ranged from 0.165 mL/min to 0.4185 mL/min, demonstrating that the ink maintained consistent flow across varying speeds.

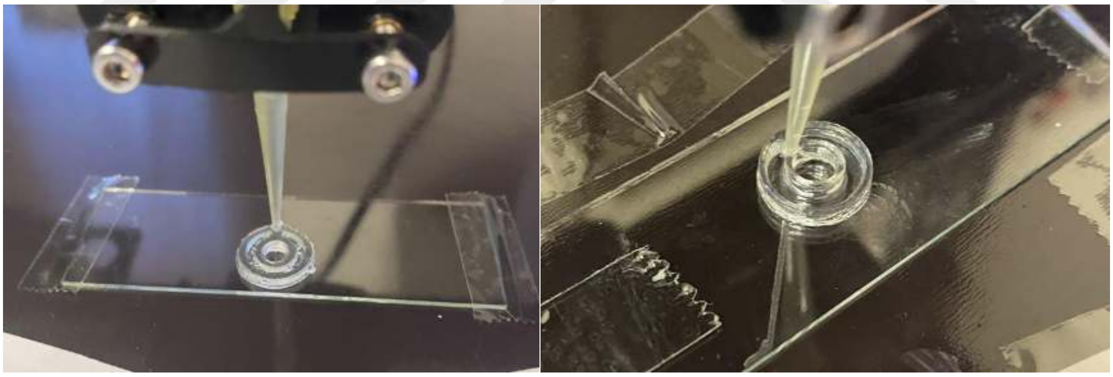

Fig. 16. Left) 13.5 mm/s printing speed. Right) 40.5 mm/s printing speed.

For print design optimization, 3D models were sliced using Cura Slicer, converting the designs into G-code. After printing and 120 minutes of gelation in ammonia vapor, a "grid" structure was produced, as seen in Figure 17**.** The inner wall thicknesses ranged from 0.63 mm to 0.9 mm, and outer walls varied from 0.9 mm to 1.1 mm. The internal grid cavities measured between 2.635 mm and 3.1 mm.

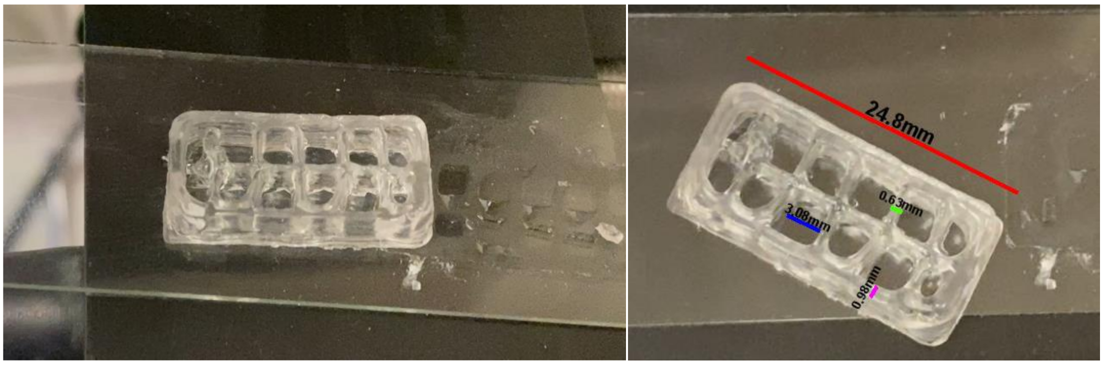

Fig. 17. Gelled grid structure after printing.

Some inconsistencies in wall thickness and shape were observed due to the limitations of Cura Slicer, which was designed for PLA and ABS filaments. These materials allow for sudden stops and retractions during extrusion, but the non-Newtonian, viscoelastic aerogel ink does not perform as well under these conditions. To address this issue, it was necessary to minimize the number of separate extrusion paths during printing.

The FullControl GCode Designer toolkit enabled manual creation of customized G-code, which allowed for better control over feature sizes and reduced the number of extrusion paths. By inputting mathematical formulas, a continuous and uninterrupted extrusion was achieved, resulting in the grid pattern shown in Figure 18, with gap sizes ranging from 0.05 mm to 0.2 mm.

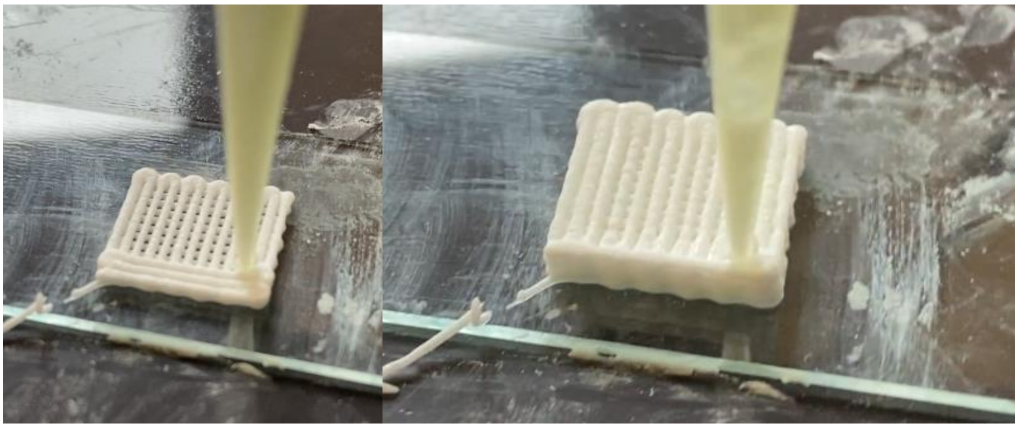

Fig. 18. TiO_2-based ink printed with manual G-code, showing gap sizes of 0.05 mm to 0.2 mm.

This section highlights how print speed, design optimization, and customized G-code contribute to overcoming the challenges of printing complex aerogel structures, enabling precise control over both print quality and structural integrity.

4.4 Rheology

Rheological measurements of the silica-TiO_2 gel were conducted at 25°C using an Anton Paar MCR 302 rheometer equipped with a 50 mm diameter 2° cone geometry. The viscosity measurements were performed under shear rates ranging from 0.01 to 1000 Hz in a shear rate sweep mode. As shown in Figure 19, the silica/TiO_2 aerogel ink exhibited shear-thinning behavior, a critical characteristic for direct ink writing applications [10][25]. This behavior ensures that the ink flows easily during extrusion but rapidly increases in viscosity post-extrusion, allowing the printed structures to maintain their shape.

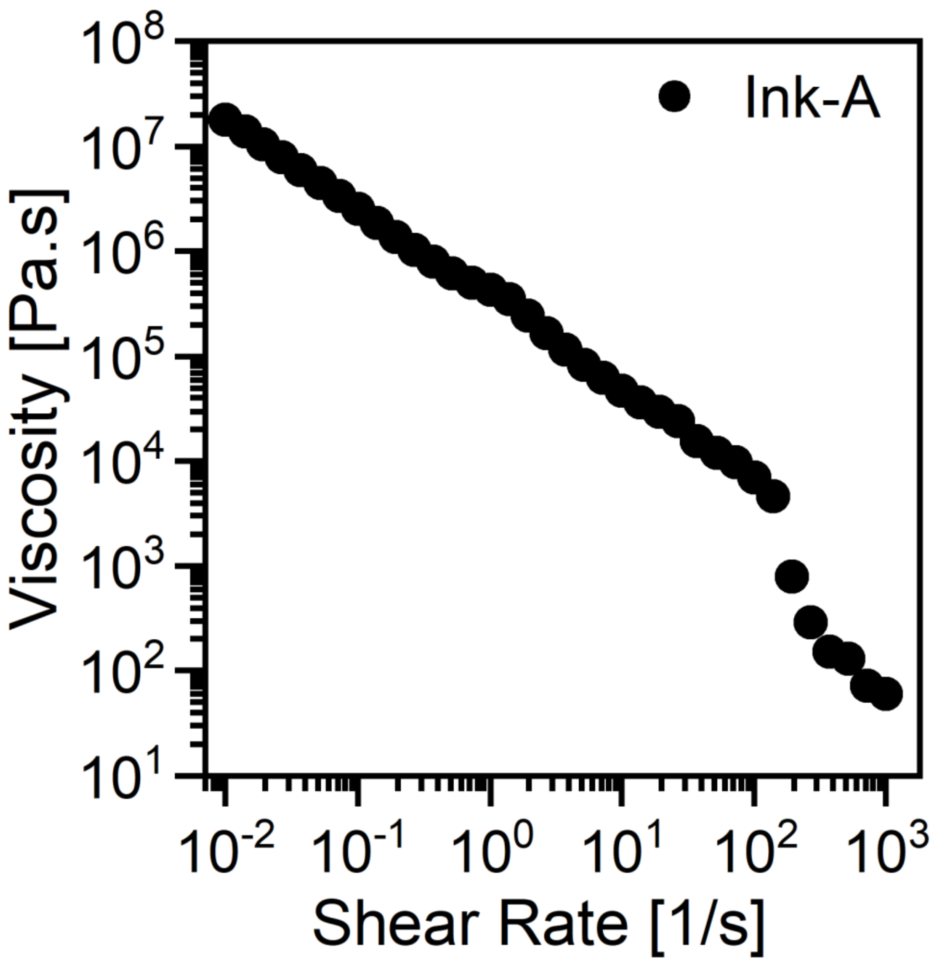

Fig. 19. The viscosity of the Silica/TiO2 gel sample as a function of shear rate.

For small amplitude oscillatory shear (SAOS) testing, an amplitude sweep was first conducted to determine the linear viscoelastic region (LVR). Subsequently, frequency sweep measurements were performed between 0.1 and 100 rad/s within the LVR. Figure 20 demonstrates the storage modulus (G') and the loss modulus (G'') for the ink sample, confirming that G' > G'' across the measured frequencies, a hallmark of gel-like materials. The material's G' and G'' remained mostly independent of frequency, further confirming its stable viscoelastic properties.

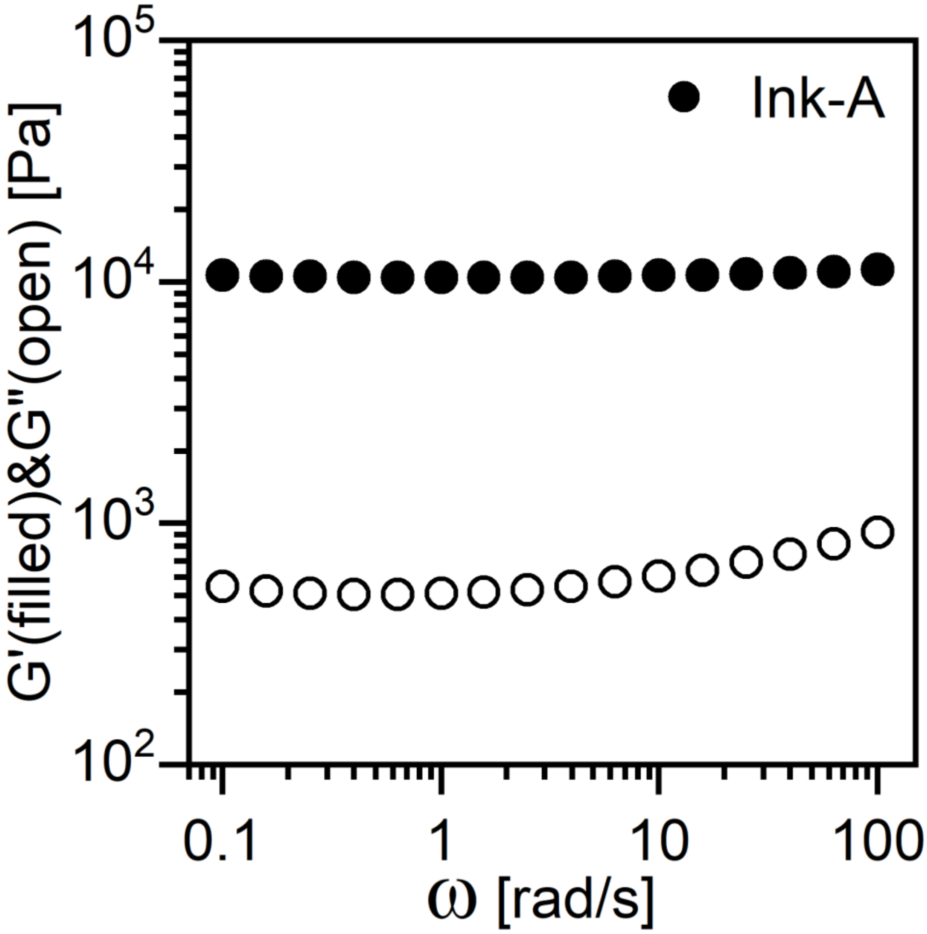

Fig. 20. Storage (G') (solid symbols) and loss (G'') (open symbols) moduli of the Silica/TiO2 gel sample.

For large amplitude oscillatory shear (LAOS) tests, conducted at 1 rad/s with strain amplitudes ranging from 0.01% to 1000%, the transition from linear to nonlinear deformation provided valuable insights into the microstructural response of the aerogel ink [26]. As shown in Figure 21, G' began to decrease with increasing strain amplitude near the LVR boundary, while G'' exhibited a peak at the critical strain (γ_0). Beyond this point, both G' and G" decreased, with G" displaying a local maximum that signals strain overshoot behavior (Type III) [25].

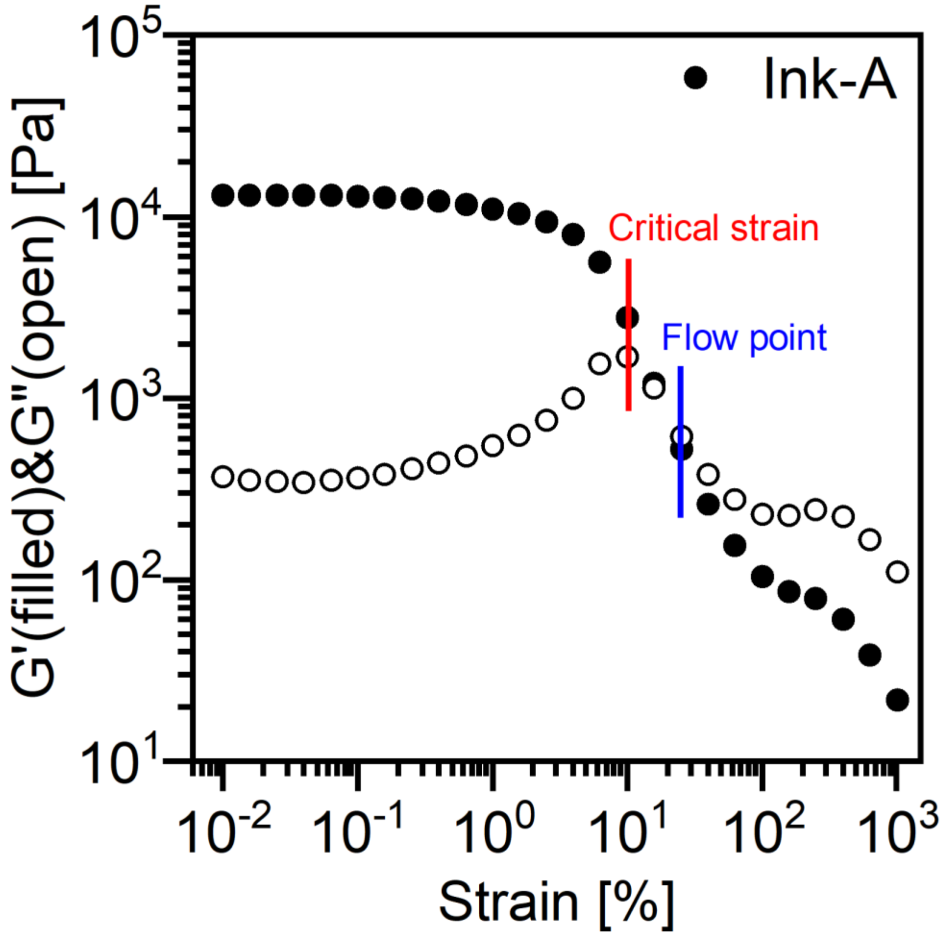

Fig. 21. The non-linear storage (G') (solid symbols) and viscous (G") (open symbols) moduli of the ink sample. The red line indicates the critical strain, and the blue line represents the flow point of the sample.

Recovery tests performed in the linear and nonlinear regions revealed partial recovery of the loss modulus after deformation, but the storage modulus did not fully recover, indicating some irreversible changes in the material's microstructure. These rheological characteristics confirm that the ink formulation is well-suited for the direct ink writing process, allowing for controlled flow during printing while ensuring mechanical stability after extrusion.

The recovery tests were performed at strain amplitudes in both the linear viscoelastic region (LVR) and the non-linear region (strain > flow point). Initially, the storage (G') and loss (G") moduli of the aerogel sample were measured at a constant angular frequency of 10 rad/s for 2 minutes in the LVR. Once a steady state was reached with no significant changes in G' and G", the strain amplitude was increased to 30%. In this non-linear viscoelastic region, the material exhibited liquid-like behavior with G" > G'. The measurement continued for an additional 5 minutes until a stable state was obtained. Following this, the strain amplitude was reduced back to lower values, equivalent to the initial 2 minutes of the test, and the measurements were continued for another 10 minutes. Although the loss modulus recovered significantly, the storage modulus did not fully recover after the large deformation phase. Figure 22 shows the storage (G', black) and viscous (G", blue) moduli of the Silica/TiO_2 gel sample. The strain amplitude during the first 2 minutes and the last 10 minutes was in the linear region (0.1%), while between the 2nd and 7th minute, the strain amplitude was in the non-linear viscoelastic region (30%).

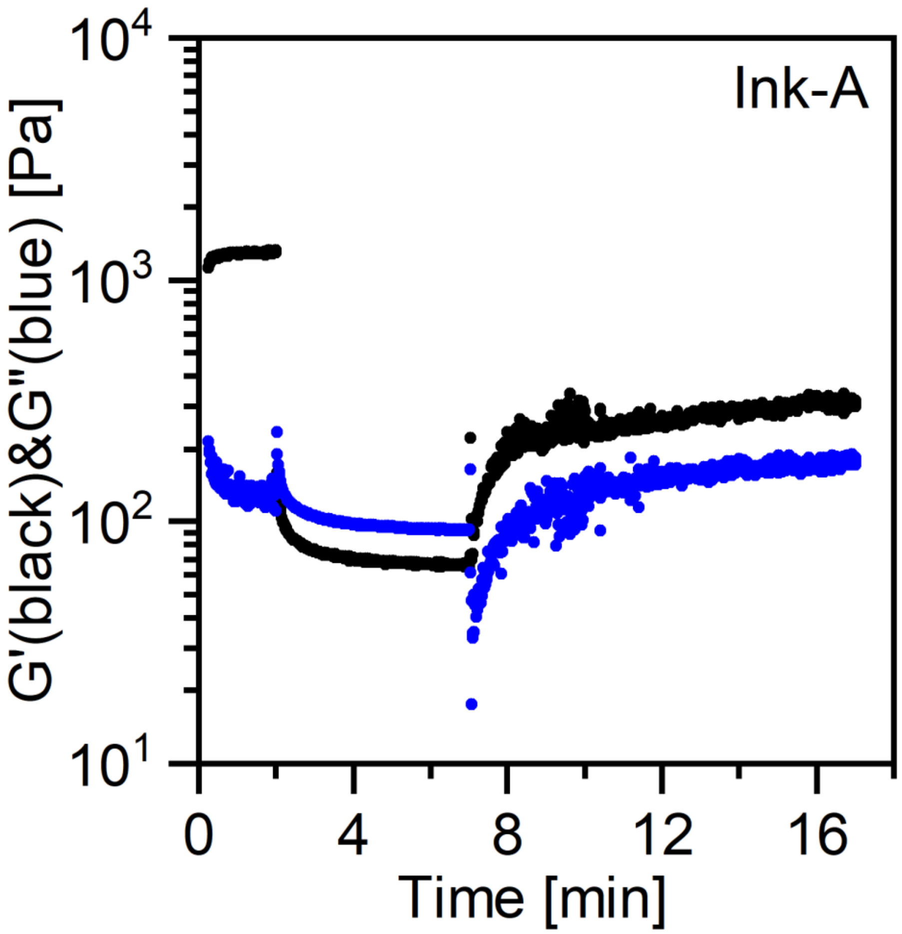

Fig. 22. Storage (G', black) and viscous (G", blue) moduli of the Silica/TiO_2 gel. The strain amplitude is in the linear region (0.1%) during the first 2 minutes and last 10 minutes, and in the non-linear region (30%) from the 2nd to 7th minute.

In summary, the rheological results show that the ink has the necessary properties for direct ink writing. Its shear-thinning behavior allows it to flow easily during printing, and the rapid increase in viscosity after extrusion helps the printed objects maintain their shape. This ensures precise control during printing and reliable outcomes for creating complex silica aerogel structures in various forms and sizes.

4.5 *Surface Area and Density*

The aerogel samples were analyzed using nitrogen absorption/desorption with a Micromeritics ASAP 2020, yielding a surface area of 407 m²/g and a density of 0.15 g/cm³. SEM images, Figure 23, show the homogeneous distribution of TiO_2 particles, ranging from 55 to 230 nm in size, within the aerogel matrix.

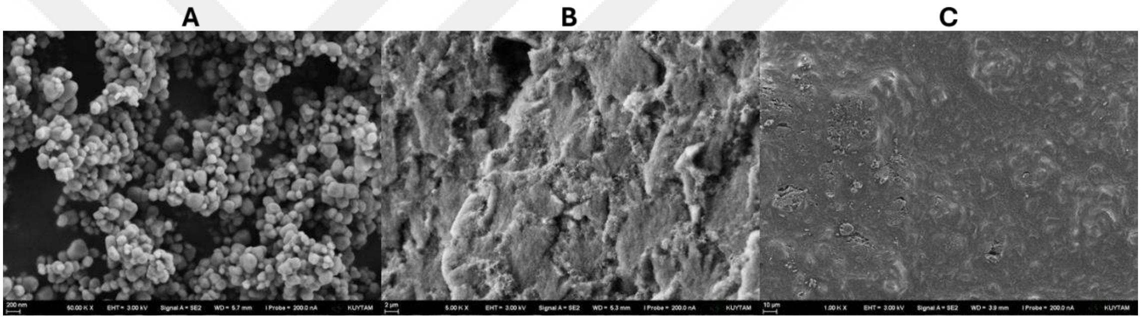

Fig. 23. SEM images of TiO_2 particles within the aerogel structure at various scales.

4.6 *Post-Processing of Printed Structures*

The post-processing of the printed aerogel structures involved several crucial steps to transform the initial prints into their final, functional forms. As shown in Figure 24, the process begins with the printing stage (1), where the ink is deposited onto the glass slide substrate. After printing, the structure is carefully removed from the glass slide and placed in an ammonia vapor chamber (A) for gelation, which lasts approximately 120 minutes. Once gelation is complete, the aerogel structures are immersed in a mixture of ethanol and isopropanol (2) to begin the solvent exchange process. The final step in the process (B) involves drying the structures in supercritical carbon dioxide at 55°C and 90 bar to preserve their delicate features and prevent shrinkage or collapse. The result is the fully dried aerogel product (3).

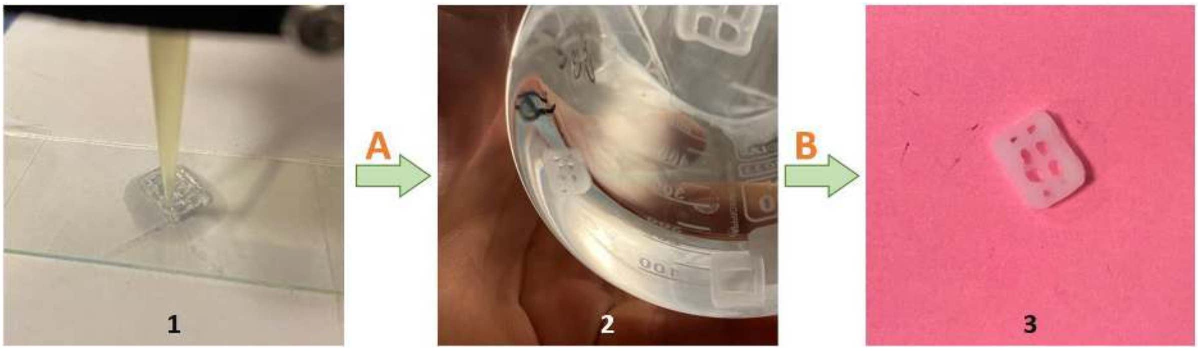

Fig. 24. Stages from printing to the final dried product.

Further processing of the printed aerogels revealed that the appearance of the final product is influenced by the percentage of TiO_2 present in the ink. As shown in Figure 25, the whiteness/opaqueness of the dried aerogel structures increases with the TiO_2 content. Prints with higher TiO_2 percentages appear whiter, indicating a direct correlation between the material composition and visual characteristics.

Fig. 25. Fully processed prints with varying TiO_2 percentages.

Once the drying process was complete, the aerogels were ready for further applications or testing. Post-processing steps, particularly gelation and supercritical CO_2 drying, were crucial in maintaining the structural integrity and fine details of the printed aerogels, as illustrated in Figure 26, where grid patterns and cylindrical structures achieved sub-millimeter precision.

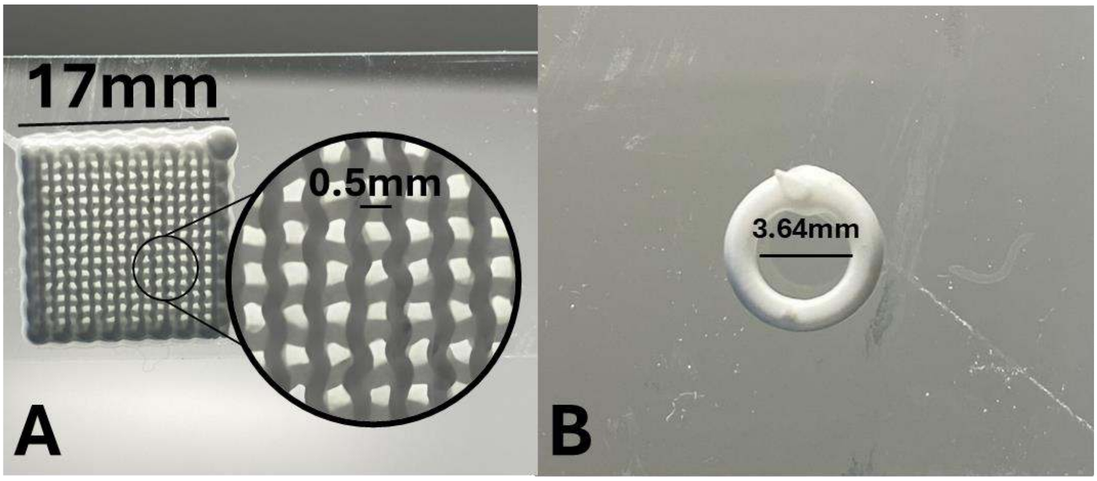

Fig. 26. A) Grid structure. B) Cylindrical structure.

These post-processing methods ensured that the aerogels retained their shape and porosity, making them suitable for various potential applications while preserving the fine structural features achieved during the printing process.

4.7 Preliminary Testing of Photocatalytic Properties

Preliminary photocatalytic testing was conducted to assess the efficacy of the 3D-printed aerogel microreactors, particularly in degrading organic pollutants under UV irradiation where the TiO_2 shows its functionality that is adds to the structure. The experimental setup utilized a cylindrical single inlet-outlet silica-TiO_2 aerogel structure due to simple and stable design, which was subjected to UV light to catalyze the breakdown of phenol in an aqueous solution. These trials, with significant contributions from Çağla Parmaksızoğlu and Defne Kuduğ, are essential to determine the baseline performance of the photocatalytic microreactors and to guide future optimizations.

4.7.1 Experimental Setup

In the initial phase of testing, the microreactor was designed and assembled with aerogel components that were carefully drilled using a handheld Dremel tool, equipped with a 1.5 mm diameter drill bit. Tygon tubing (Cole Palmer; i.d. = 0.5 mm, o.d. = 1.52 mm) was inserted into the drilled holes to allow fluid flow through the reactor. The aerogels were then secured between two standard glass microscope slides using an epoxy adhesive, which provided both moisture insulation and additional structural reinforcement. The complete epoxy coating also enhanced the mechanical stability of the aerogels, which otherwise are fragile due to their porous nature.

For the photocatalytic testing, an LED setup was constructed using components from Thorlabs. The light source was a UV LED flashlight with a wavelength of 365 nm, and the light was focused onto the microreactor using a Thorlabs LA1384-A lens. This setup ensured that the UV light was concentrated along the central axis of the microreactor, maximizing exposure to the aerogel's surface. The microreactor was meticulously aligned with both the lens and the LED to ensure optimal light delivery to the photocatalytic material. The experimental setup can be seen in Figure 27.

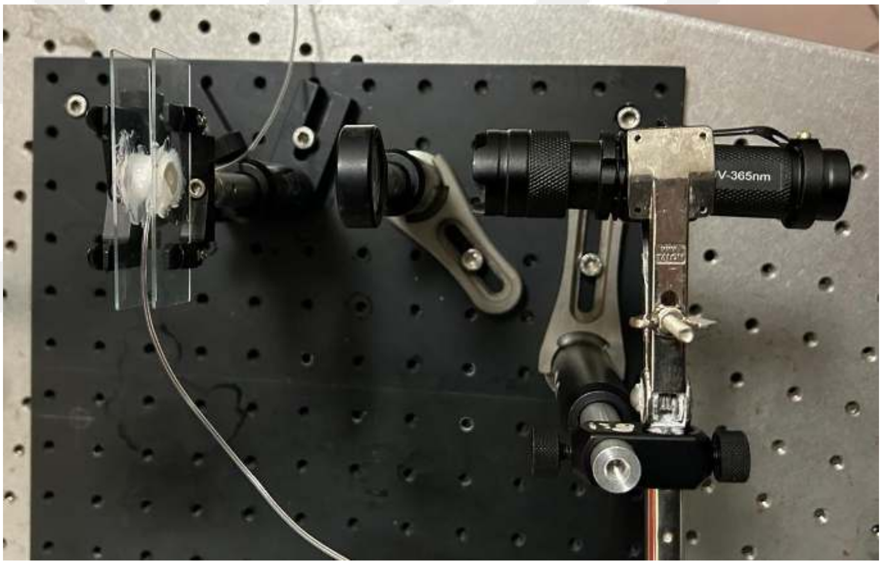

Fig. 27. The LED setup with a cylindrical tube silica aerogel microreactor sample mounted.

With this setup, the photocatalytic trials involved passing a pre-prepared 331.5 µM phenol solution through the microreactor at a controlled flow rate of 50 µL/min using a syringe pump. The phenol solution was introduced via the tubing, allowing it to interact with the aerogel surface within the reactor while being exposed to the UV light. Samples were collected at regular 5-minute intervals over a 160-minute period and were immediately shielded from ambient light by covering them with aluminum foil to prevent any unintended photoreactions.

4.7.2 *Analysis and Observations*

The samples were analyzed using a UV-Vis spectrophotometer (Thermo Fischer Nanodrop 2000) set between 190 nm and 640 nm, with a focus on measuring absorbance at 270 nm, the characteristic absorption peak for phenol. Throughout the experiment, the absorbance values remained relatively stable around 0.052, which closely matched the initial phenol concentration of 0.0502. The measurement can be seen in Figure 28. These results indicated no significant photocatalytic degradation of the phenol under the tested conditions.

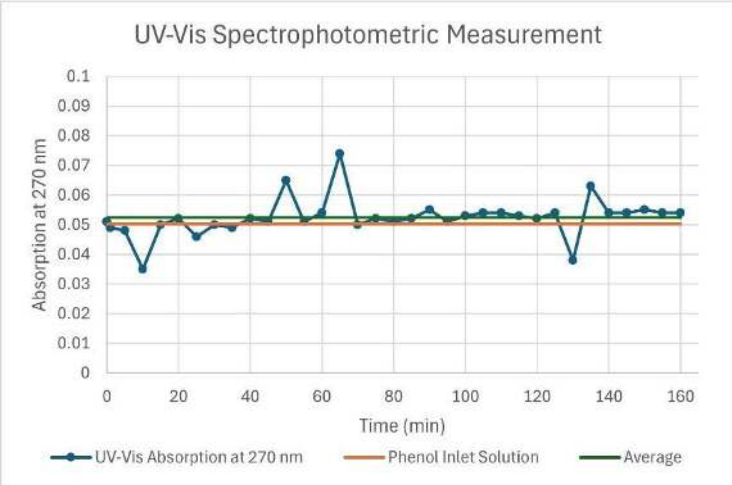

Fig. 28. UV-Vis spectrophotometric absorbance measurements at 270 nm were conducted on samples from Microreactor-2, collected at 5-minute intervals over a total duration of 160 minutes.

4.7.3 *Discussion of Potential Improvements*

Several factors likely contributed to the limited photocatalytic activity observed in the initial trials:

1. **UV Light Intensity**: The UV LED flashlight may not have provided sufficient power to activate the TiO_2 photocatalyst embedded in the aerogel. Future tests should explore using a more powerful or focused light source to ensure adequate energy reaches the catalyst.
2. **Epoxy Insulation**: The complete epoxy coating, while providing structural support, might have blocked some of the UV light, preventing it from reaching the TiO_2

particles on the aerogel surface. Reducing or strategically applying the epoxy layer could improve light penetration.

3. **Flow Rate**: The flow rate of 50 µL/min may have been too high for optimal contact between the phenol solution and the photocatalytic aerogel surface. Slower flow rates could extend the reaction time, allowing for more effective interaction and degradation.
4. **Hydrophobic Surface Properties**: The hydrophobic nature of the aerogel, with a measured contact angle of 119.8°, could have inhibited proper contact between the phenol solution and the aerogel surface. Modifying the surface treatment to reduce hydrophobicity might improve photocatalytic efficiency.

4.8 Refractive Index, TIR, and Waveguiding in Aerogels

The refractive index of aerogels plays a critical role in their suitability for optofluidic applications, particularly for waveguiding and light confinement by total internal reflection (TIR). The low refractive index of aerogels, combined with their highly porous structure, makes them an excellent candidate for cladding in liquid-core waveguides.

The refractive index n of aerogels is directly related to their density ρ, as demonstrated by various empirical correlations [27][28][29][30]. For silica aerogels, the refractive index typically follows the linear relationship:

$$n = 1 + k\rho$$

where k is the proportionality constant and typically falls within the range of 0.206 0.270 cm³/g, depending on the specific conditions of their preparation [27][29][31] [32][33][34]. Studies indicate that for silica aerogels with densities ranging from 0.15 to 0.39 g/cm³, the refractive index remains below 1.1, which is significantly lower than the refractive index of water $n_{H_2O} = 1.33$.

For our aerogel with a density of 0.15 g/cm³, the refractive index has been measured at approximately 1.023, making it an ideal cladding material for TIR-based waveguides.

According to Snell's law, TIR occurs when light traveling through a medium with a higher refractive index is incident at the boundary with a medium of lower refractive index, beyond the critical angle θ_c, which is defined as:

$$\theta_c = \arcsin\left(\frac{n_{caldding}}{n_{core}}\right)$$

In the case of our aerogel-based optofluidic waveguides, the core liquid (e.g., water) has a refractive index of 1.33, and the aerogel cladding, with its refractive index of 1.023, allows for efficient TIR. The theoretical calculated critical angle for the aerogel cladding is approximately 50.1°.

4.8.1 Total Internal Reflection and Waveguiding Efficiency

Waveguiding efficiency is closely linked to the refractive index contrast between the core and cladding materials. For multimode optofluidic waveguides, the numerical aperture (NA) provides a measure of the light-gathering ability. The NA is given by [35]:

$$NA = \sqrt{{n_{core}}^2 - {n_{caldding}}^2}$$

For the aerogel with a density of 0.15 g/cm³, the NA is calculated to be 0.85, which is significantly higher than typical doped silica fibers (NA ≈ 0.37) and Teflon-coated optical fibers (NA ≈ 0.66) [36]. This high NA allows for efficient light coupling and broad-angle light distribution

These findings regarding the refractive index and NA of the printed aerogel structures not only demonstrate their exceptional suitability for waveguiding applications, offering better light confinement and coupling efficiency compared to conventional materials, but also highlight the flexibility of their properties. This adaptability allows for further optimization and tuning, making these aerogels versatile candidates for a wide range of optofluidic and photonic applications, where precise control over light propagation is crucial.

Chapter 5:
CONCLUSION

The development of a customized 3D printing system for fabricating aerogels with functional additives represents a significant advancement in the fields of additive manufacturing and materials science. By integrating a modified Creality Ender 3 Pro printer with a custom-designed syringe pump system, this research successfully addressed the limitations of conventional fused deposition modeling (FDM) techniques, which are not suited for printing non-solid, highly viscous materials such as aerogels. The combination of hardware and software innovations provided precise control over extrusion and enhanced the overall print quality, enabling the production of intricate aerogel structures with improved mechanical properties and stability.

A critical challenge encountered during this process was the formation of air pockets within the syringe, which led to extrusion inconsistencies and defects in the printed structures. By implementing a systematic approach to air pocket removal, we ensured a homogeneous ink mixture, which significantly improved print reliability and structural integrity. This solution not only enhanced the overall quality of the aerogel constructs but also enabled the production of more complex geometries.

The rheological characterization of the aerogel ink revealed its essential shear-thinning behavior, which facilitated smoother extrusion and allowed for rapid recovery of viscosity post-printing. This rheological profile is crucial for maintaining the shape and precision of the printed structures. Moreover, the successful incorporation of titanium dioxide (TiO_2) as an additive demonstrated the versatility of 3D-printed aerogels for functional applications, particularly in environmental remediation. The photocatalytic properties of TiO_2, combined with the aerogel's large surface area and porous structure, position this material for applications in water purification, air filtration, and catalysis.

Surface area and density measurements, coupled with SEM analysis, confirmed the homogeneous dispersion of TiO_2 within the aerogel matrix, validating the effectiveness of the ink formulation. The aerogel structures displayed high precision, excellent stability, and enhanced functional properties, which are crucial for their intended applications.

This research not only showcases the potential of 3D printing as a scalable, cost-effective solution for producing aerogels with tailored properties but also highlights its broad applicability across various sectors, including catalysis, thermal insulation, and environmental sustainability. The use of commercially available components and open-source software further enhances the accessibility of this approach, making it a practical option for research institutions and industries alike.

Future research directions will focus on optimizing the formulation of aerogel inks with a wider range of functional additives, refining printing parameters to further improve resolution and performance, and scaling up the production process for industrial applications. Additionally, exploring new applications such as optofluidic microreactors for photocatalytic processes and conducting a comprehensive assessment of the environmental impact of the production process will help realize the full potential of 3D-printed aerogels. By addressing these areas, this research paves the way for further advancements in additive manufacturing and the development of multifunctional aerogel-based materials.

BIBLIOGRAPHY

[1] N. R. Khan, T. Sharmin, and A. Bin Rashid, "Exploring the Versatility of Aerogels: Broad Applications in Biomedical Engineering, Astronautics, Energy Storage, Biosensing, and Current Progress," *Heliyon*. 2024.

[2] J. Lin, G. Li, W. Liu, R. Qiu, H. Wei, K. Zong, and X. Cai, "A review of recent progress on the silica aerogel monoliths: synthesis, reinforcement, and applications," *Journal of Materials Science*. 2021.

[3] Q. Zhang, F. Zhang, S. P. Medarametla, H. Li, C. Zhou, and D. Lin, "3D Printing of Graphene Aerogels," *Small*, 2016.

[4] H. Maleki, L. Durães, and A. Portugal, "An overview on silica aerogels synthesis and different mechanical reinforcing strategies," *J. Non. Cryst. Solids*, 2014.

[5] N. Hüsing and U. Schubert, "Aerogels - Airy Materials: Chemistry, Structure, and Properties," *Angewandte Chemie - International Edition*. 1998.

[6] V. C. F. Li, C. K. Dunn, Z. Zhang, Y. Deng, and H. J. Qi, "Direct Ink Write (DIW) 3D Printed Cellulose Nanocrystal Aerogel Structures," *Sci. Rep.*, 2017.

[7] J. Yang, H. Wang, B. Zhou, J. Shen, Z. Zhang, and A. Du, "Versatile Direct Writing of Aerogel-Based Sol-Gel Inks," *Langmuir*, 2021.

[8] Y. Jiang, Z. Xu, T. Huang, Y. Liu, F. Guo, J. Xi, W. Gao, and C. Gao, "Direct 3D Printing of Ultralight Graphene Oxide Aerogel Microlattices," *Adv. Funct. Mater.*, 2018.

[9] N. M. Bakhori, Z. Ismail, M. Z. Hassan, and R. Dolah, "Emerging Trends in Nanotechnology: Aerogel-Based Materials for Biomedical Applications," *Nanomaterials*. 2023.

[10] S. Zhao, G. Siqueira, S. Drdova, D. Norris, C. Ubert, A. Bonnin, S. Galmarini, M. Ganobjak, Z. Pan, S. Brunner, G. Nyström, J. Wang, M. M. Koebel, and W. J. Malfait, "Additive manufacturing of silica aerogels," *Nature*, 2020.

[11] R. Wordsworth, L. Kerber, and C. Cockell, "Enabling Martian habitability with silica aerogel via the solid-state greenhouse effect," *Nature Astronomy*. 2019.

[12] G. Eris, D. Sanli, Z. Ulker, S. E. Bozbag, A. Jonás, A. Kiraz, and C. Erkey, "Three-dimensional optofluidic waveguides in hydrophobic silica aerogels via supercritical fluid processing," *J. Supercrit. Fluids*, 2013.

[13] Y. Özbakır, A. Jonáš, A. Kiraz, and C. Erkey, "A new type of microphotoreactor

with integrated optofluidic waveguide based on solid-air nanoporous aerogels," *R. Soc. Open Sci.*, 2018.

[14] S. Zhao, W. J. Malfait, N. Guerrero-Alburquerque, M. M. Koebel, and G. Nyström, "Biopolymer Aerogels and Foams: Chemistry, Properties, and Applications," *Angewandte Chemie - International Edition*. 2018.

[15] G. M. Pajonk, E. Elaloui, P. Achard, B. Chevalier, J. L. Chevalier, and M. Durant, "Physical properties of silica gels and aerogels prepared with new polymeric precursors," *J. Non. Cryst. Solids*, 1995.

[16] Y. Özbakır, A. Jonáš, A. Kiraz, and C. Erkey, "An aerogel-based photocatalytic microreactor driven by light guiding for degradation of toxic pollutants," *Chem. Eng. J.*, 2021.

[17] M. Liu, L. Gan, Y. Pang, Z. Xu, Z. Hao, and L. Chen, "Synthesis of titania-silica aerogel-like microspheres by a water-in-oil emulsion method via ambient pressure drying and their photocatalytic properties," *Colloids Surfaces A Physicochem. Eng. Asp.*, 2008.

[18] S. Baas and V. Saggiomo, "Ender3 3D printer kit transformed into open, programmable syringe pump set," *HardwareX*, 2021.

[19] S. Garzon-Hernandez, D. Garcia-Gonzalez, A. Jérusalem, and A. Arias, "Design of FDM 3D printed polymers: An experimental-modelling methodology for the prediction of mechanical properties," *Mater. Des.*, vol. 188, p. 108414, 2020.

[20] X. Chen, X. Ye, J. He, L. Pan, S. Xu, and C. Xiong, "Preparation of Fe3+-doped TiO2 aerogels for photocatalytic reduction of CO2 to methanol," *J. Sol-Gel Sci. Technol.*, 2020.

[21] C. A. García-González, M. C. Camino-Rey, M. Alnaief, C. Zetzl, and I. Smirnova, "Supercritical drying of aerogels using CO 2: Effect of extraction time on the end material textural properties," *J. Supercrit. Fluids*, 2012.

[22] B. Bhushan and M. Caspers, "An overview of additive manufacturing (3D printing) for microfabrication," *Microsyst. Technol.*, 2017.

[23] V. Štengl, S. Bakardjieva, J. Šubrt, and L. Szatmary, "Titania aerogel prepared by low temperature supercritical drying," *Microporous Mesoporous Mater.*, 2006.

[24] W. J. Malfait, S. Zhao, R. Verel, S. Iswar, D. Rentsch, R. Fener, Y. Zhang, B. Milow, and M. M. Koebel, "Surface Chemistry of Hydrophobic Silica Aerogels," *Chem. Mater.*, 2015.

[25] C. Zhu, T. Y. J. Han, E. B. Duoss, A. M. Golobic, J. D. Kuntz, C. M. Spadaccini, and M. A. Worsley, “Highly compressible 3D periodic graphene aerogel microlattices,” *Nat. Commun.*, 2015.

[26] K. Hyun, M. Wilhelm, C. O. Klein, K. S. Cho, J. G. Nam, K. H. Ahn, S. J. Lee, R. H. Ewoldt, and G. H. McKinley, “A review of nonlinear oscillatory shear tests: Analysis and application of large amplitude oscillatory shear (LAOS),” *Progress in Polymer Science (Oxford)*. 2011.

[27] M. Cantin, M. Casse, L. Koch, R. Jouan, P. Mestreau, D. Roussel, F. Bonnin, J. Moutel, and S. J. Teichner, “Silica aerogels used as Cherenkov radiators,” *Nucl. Instruments Methods*, 1974.

[28] Y. K. Akimov, “Fields of application of aerogels (review),” *Instruments and Experimental Techniques*. 2003.

[29] S. Henning and L. Svensson, “Production of silica aerogel,” *Phys. Scr.*, 1981.

[30] A. Buzykaev, A. Danilyuk, S. Ganzhur, T. Gorodetskaya, E. Kravchenko, A. Onuchin, and A. Vorobiov, “Aerogels with high optical parameters for Cherenkov counters,” *Nucl. Instruments Methods Phys. Res. Sect. A Accel. Spectrometers, Detect. Assoc. Equip.*, 1996.

[31] Y. özbakir, A. Jonas, A. Kiraz, and C. Erkey, “Aerogels for optofluidic waveguides,” *Micromachines*. 2017.

[32] G. Poelz and R. Riethmüller, “Preparation of silica aerogel for Cherenkov counters,” *Nucl. Instruments Methods*, 1982.

[33] P. Wang, A. Beck, W. Körner, A. Beck, and A. Beck, “Density and refractive index of silica aerogels after low- and high-temperature supercritical drying and thermal treatment,” *J. Phys. D. Appl. Phys.*, 1994.

[34] A. F. Danilyuk, V. L. Kirillov, M. D. Savelieva, V. S. Bobrovnikov, A. R. Buzykaev, E. A. Kravchenko, A. V. Lavrov, and A. P. Onuchin, “Recent results on aerogel development for use in Cherenkov counters,” in *Nuclear Instruments and Methods in Physics Research, Section A: Accelerators, Spectrometers, Detectors and Associated Equipment*, 2002.

[35] B. Yalizay, Y. Morova, K. Dincer, Y. Ozbakir, A. Jonas, C. Erkey, A. Kiraz, and S. Akturk, “Versatile liquid-core optofluidic waveguides fabricated in hydrophobic silica aerogels by femtosecond-laser ablation,” *Opt. Mater. (Amst).*, 2015.

[36] N. A. Issa, “High numerical aperture in multimode microstructured optical fibers,” *Appl. Opt.*, 2004.

APPENDIX

Appendix 1: Python Calibration GUI Code

```
import serial
import time
from tkinter import *
from PIL import ImageTk, Image

# Create main window
root = Tk()
root.title("3D Printer Controller")
root.iconbitmap("H:/My Drive/3D Print Project/Python/images/KirazLab_logo.ico")

# Display banner image
banner = ImageTk.PhotoImage(Image.open("H:/My Drive/3D Print Project/Python/images/rsz_kirazlabbanner.png").resize((600, 225), Image.ANTIALIAS))
bannerLabel = Label(image=banner)
bannerLabel.grid(row=0, column=0, sticky="ewns")

#########################################################################################################
# Frame for Connection Status and Command

statusFrame = LabelFrame(root, text="Connection Status and Command")
statusFrame.grid(row=0, column=1, sticky="ewns")

# Connection Check and Port Allocation
MAX_BUFF_LEN = 255
SETUP = False
port = None
```

```
prev = time.time()
while not SETUP:
    try:
        port = serial.Serial("COM3", 115200, timeout=1)  # COM3 is my 3D printer's
connection port
    except:
        if time.time() - prev > 2:
            print("No serial detected, please plug 3D printer")
            prev = time.time()
    if port is not None:
        SETUP = True
        Connected = Label(statusFrame, text="Connected!").grid(row=0, column=0,
columnspan=2, sticky="ew")

# Function to send custom G-code commands
def sendCommand():
    write_ser(commandValue.get())
    commandLabel = Label(statusFrame, text=commandValue.get()).grid(row=4,
column=0, columnspan=2, sticky="ew")

# Function to home the printer axis
def homeAxis():
    write_ser("G28")
    homeLabel = Label(statusFrame, text="Homing Axis").grid(row=4, column=0,
columnspan=2, sticky="ew")

# Serial communication functions for reading and writing
def read_ser(num_char=1):
    string = port.read(num_char)
    return string.decode()

def write_ser(cmd):
```

```
        cmd = cmd + '\n'
        port.write(cmd.encode())

    # Input field for sending custom G-code commands
    commandValue = Entry(statusFrame, borderwidth=5)
    commandValue.insert(0, "Enter Command")
    commandValue.grid(row=3, column=0)

    # Buttons for sending commands and homing axis
    homeButton = Button(statusFrame, text="Home Axis",
command=homeAxis).grid(row=2, column=0, columnspan=2, sticky="ew")
    commandButton = Button(statusFrame, text="Send Command",
command=sendCommand).grid(row=3, column=1, sticky="ew")

    ##################################################################
####################################
    # Frame for Variables and Conditions

    variableFrame = LabelFrame(root, text="Variables and Conditions", padx=25,
pady=25)
    variableFrame.grid(row=1, column=0, sticky="ewns")

    enterFLabel = Label(variableFrame, text="Enter F Value: ").grid(row=1,
column=0, sticky="ew")
    enterELabel = Label(variableFrame, text="Enter E Value: ").grid(row=2,
column=0, sticky="ew")

    fSpeedValue = Entry(variableFrame, borderwidth=5)
    fSpeedValue.grid(row=1, column=1)

    eStepsValue = Entry(variableFrame, borderwidth=5)
    eStepsValue.grid(row=2, column=1)
```

```
    setConLabel = Label(variableFrame, text="Initial Conditions Not
Set!").grid(row=0, column=3, sticky="ew")

    # Function to set initial conditions
    def setInitialConditions():
        write_ser("M302 S0")
        write_ser("M83")
        setLabel = Label(variableFrame, text="Initial Conditions Set!").grid(row=0,
column=3, sticky="ew")

    # Functions to set F speed and E steps
    def fSpeed():
        write_ser("G0 F" + fSpeedValue.get())
        fSpeedLabel = Label(variableFrame, text="F set to " +
fSpeedValue.get()).grid(row=1, column=3, sticky="ew")

    def eSteps():
        write_ser("M92 E" + eStepsValue.get())
        eStepsLabel = Label(variableFrame, text="E set to " +
eStepsValue.get()).grid(row=2, column=3, sticky="ew")

    # Buttons for setting initial conditions, F speed, and E steps
    initialConditions = Button(variableFrame, text="Set initial conditions",
command=setInitialConditions).grid(row=0, column=0, columnspan=3, sticky="ew")
    fSpeedButton = Button(variableFrame, text="Set F value",
command=fSpeed).grid(row=1, column=2, sticky="ew")
    eStepsButton = Button(variableFrame, text="Set E Value",
command=eSteps).grid(row=2, column=2, sticky="ew")

    ######################################################################
####################################
    # Frame for Extrusion Control
```

```
    extrudeFrame = LabelFrame(root, text="Extrusion control", padx=25, pady=25)
    extrudeFrame.grid(row=1, column=1, sticky="ewns")

    extrudeValue = Entry(extrudeFrame, borderwidth=5)
    extrudeValue.insert(0, "Amount")
    extrudeValue.grid(row=1, column=0, sticky="ew")

    emptyLabel = Label(extrudeFrame, text="").grid(row=3, column=0, sticky="ew")

    # Functions for extruding and retracting filament
    def extrude():
        write_ser("G1 E" + extrudeValue.get())
        extrudeLabel = Label(extrudeFrame, text="Extruding " + extrudeValue.get() + "
ml").grid(row=3, column=0, sticky="ew")

    def retract():
        write_ser("G1 E-" + extrudeValue.get())
        retractLabel = Label(extrudeFrame, text="Retracting " + extrudeValue.get() + "
ml").grid(row=3, column=0, sticky="ew")

    # Buttons for extruding and retracting
    extrudeButton = Button(extrudeFrame, text="Extrude",
command=extrude).grid(row=0, column=0, sticky="ew")
    retractButton = Button(extrudeFrame, text="Retract",
command=retract).grid(row=2, column=0, sticky="ew")

    ######################################################################
####################################
    # Frame for Linear Movement

    global xCoord
    global yCoord
    global zCoord
```

```
xCoord = 0
yCoord = 0
zCoord = 0

movementFrame = LabelFrame(root, text="Linear Movement", padx=25, pady=25)
movementFrame.grid(row=0, column=2, sticky="ewns")

movementStepValue = Entry(movementFrame, borderwidth=5)
movementStepValue.insert(0, "Enter Step")
movementStepValue.grid(row=1, column=1)

# Functions for moving in X, Y, and Z directions
def lineerXMove(xCoord):
    write_ser("G0 X" + movementStepValue.get())
    xCoord = xCoord + float(movementStepValue.get())
    strXcoord = "X: " + str(xCoord)
    movementXLabel = Label(movementFrame, text=strXcoord).grid(row=3,
column=0, columnspan=2, sticky="ew")
    return xCoord

def lineeriXMove(xCoord):
    write_ser("G0 X-" + movementStepValue.get())
    xCoord = xCoord - float(movementStepValue.get())
    strXcoord = "X: " + str(xCoord)
    movementXLabel = Label(movementFrame, text=strXcoord).grid(row=3,
column=0, columnspan=2, sticky="ew")
    return xCoord

def lineerYMove(yCoord):
    write_ser("G0 Y" + movementStepValue.get())
    yCoord = yCoord + float(movementStepValue.get())
    strYcoord = "Y: " + str(yCoord)
```

```
        movementYLabel = Label(movementFrame, text=strYcoord).grid(row=4,
column=0, columnspan=2, sticky="ew")
        return yCoord

    def lineeriYMove(yCoord):
        write_ser("G0 Y-" + movementStepValue.get())
        yCoord = yCoord - float(movementStepValue.get())
        strYcoord = "Y: " + str(yCoord)
        movementYLabel = Label(movementFrame, text=strYcoord).grid(row=4,
column=0, columnspan=2, sticky="ew")
        return yCoord

    def lineerZMove(zCoord):
        write_ser("G0 Z" + movementStepValue.get())
        zCoord = zCoord + float(movementStepValue.get())
        strZcoord = "Z: " + str(zCoord)
        movementYLabel = Label(movementFrame, text=strZcoord).grid(row=5,
column=0, columnspan=2, sticky="ew")
        return zCoord

    def lineeriZMove(zCoord):
        write_ser("G0 Z-" + movementStepValue.get())
        zCoord = zCoord - float(movementStepValue.get())
        strZcoord = "Z: " + str(zCoord)
        movementYLabel = Label(movementFrame, text=strZcoord).grid(row=5,
column=0, columnspan=2, sticky="ew")
        return zCoord

    # Buttons for linear movement along X, Y, and Z axes
    yUpButton = Button(movementFrame, text="Y Up", command=lambda:
lineerYMove(yCoord)).grid(row=0, column=1, sticky="ew")
    yDownButton = Button(movementFrame, text="Y Down", command=lambda:
lineeriYMove(yCoord)).grid(row=2, column=1, sticky="ew")
```

```
    xRightButton = Button(movementFrame, text="X Right", command=lambda:
lineerXMove(xCoord)).grid(row=1, column=2, sticky="ew")
    xLeftButton = Button(movementFrame, text="X Left", command=lambda:
lineeriXMove(xCoord)).grid(row=1, column=0, sticky="ew")
    zUpButton = Button(movementFrame, text="Z Up", command=lambda:
lineerZMove(zCoord)).grid(row=0, column=2, sticky="ew")
    zDownButton = Button(movementFrame, text="Z Down", command=lambda:
lineeriZMove(zCoord)).grid(row=2, column=2, sticky="ew")

    ####################################################################
#####################################
    # Key Binds for faster controls

    root.bind('<Return>', lambda event: sendCommand())
    root.bind('<Up>', lambda event: extrude())
    root.bind('<Down>', lambda event: retract())

    Grid.rowconfigure(root, 0, weight=1)
    Grid.columnconfigure(root, 0, weight=1)

    ####################################################################
#####################################
    # Calibration Window

    def calibrateWindow():
        window = Toplevel(root)
        window.title("Calibration")
        window.iconbitmap("H:/My Drive/3D Print Project/Python/images/target.ico")
        warningLabel = Label(window, text="!! Make sure you have at least 12ml !!",
fg="red").grid(row=0, column=0, columnspan=3, sticky="ew")
        extrudedAmount = Entry(window, borderwidth=5)
        extrudedAmount.insert(0, "Enter Amount Extruded")
        extrudedAmount.grid(row=1, column=2, sticky="ew")
```

```
        preCal_eStepsValue = Entry(window, borderwidth=5)
        preCal_eStepsValue.insert(0, "Enter E steps value")
        preCal_eStepsValue.grid(row=1, column=0, sticky="ew")

        # Extrude for calibration
        def extrudeCalibration():
            write_ser("M302 S0")
            write_ser("M83")
            write_ser("G0 F5")
            write_ser("M92 E" + str(preCal_eStepsValue.get()))
            write_ser("G1 E2")
            extrudeCalLabel = Label(window, text="Extruding 2 ml").grid(row=2,
column=0, columnspan=3, sticky="ew")

        # Calculate new E steps value based on extruded amount
        def calibrationCalculation():
            new_eStepsValue = float(preCal_eStepsValue.get()) /
(float(extrudedAmount.get()) / 2)
            new_eSteps = Label(window, text="Updated E steps value is: " +
str(new_eStepsValue)).grid(row=1, column=4, sticky="ew")

        extrudeCalibrationButton = Button(window, text="1. Extrude 2ml",
command=extrudeCalibration).grid(row=1, column=1, sticky="ew")
        calibrationButton = Button(window, text="2. Calibrate (new value)",
command=calibrationCalculation).grid(row=1, column=3, sticky="ew")

    # Button to open calibration window
    calibrateButton = Button(statusFrame, text="Calibrate",
command=calibrateWindow).grid(row=1, column=0, columnspan=2, sticky="ew")

    ######################################################################
####################################
    # Main event loop
```

```
root.mainloop()
```

Appendix 2: Versions of Syringe Pump

Developing the syringe pump took 3 editions as seen below.

The 1st edition had limited modularity. Syringe size was fixed, and the frame was heavier than the future editions. In addition, due to the stepper motor and T8 lead screw places at the rear the force was not normal to the syringe thus leading the top of the syringe being unevenly pressured. Having and extra set of steel rods with bearings did not solve the problem. Another approach was needed to convey the force from the motor to the syringe leading to the next edition.

The 2nd edition was implemented via cogs to convert the rotational force of the stepper motor to the syringe. This design was promising but still had the two steel rods to keep the slider on trach and leading to occasional force distribution problems and extra weight.

The 3rd edition solves the previous issues by removing the guiding steel rods and placing the T8 lead screw on the syringe. The lead screw was modified to have an adapter that connects the syringe directly to the screw. In addition, the frame was made to fit many sizes of syringes easily.

Appendix 3: FullControl GCode example

The figure below shows an example sheet made to print a simple cylindrical structure via the FullControl GCode. This tool, based on excel sheets, converts simple functions/commands to GCode that is read by the 3D printer.

Design ID:	Soft Grid Auto Adjust	**Save to sheet:**	First Test								
Feature											
1	Line	Cartesian	50.5	50	0	75.5	50	0	Print	0.4	0.3
2	Circle/arc	75.5	50.5	0	0.5	270	180	anti-CW	100	0.4	0.3
3	Line	Cartesian	75.5	51	0	50.5	51	0	Print	0.4	0.3
4	Circle/arc	50.5	51.5	0	0.5	270	180	CW	100	0.4	0.3
5	Cartesian repeat	1-4	0	2	0	12					
6	Line	Cartesian	50.5	76	0	76	76	0	Print	0.4	0.3
7	Line	Cartesian	76	75.5	0.33	76	50.5	0.33	Print	0.4	0.3
8	Circle/arc	75.5	50.5	0.33	0.5	0	180	CW	100	0.4	0.3
9	Line	Cartesian	75	50.5	0.33	75	75.5	0.33	Print	0.4	0.3
10	Circle/arc	74.5	75.5	0.33	0.5	0	180	anti-CW	100	0.4	0.3
11	Cartesian repeat	7-10	-2	0	0	12					
12	Line	Cartesian	50	75.5	0.33	50	50	0.33	Print	0.4	0.3
13	Cartesian repeat	1-12	0	0	0.66	15					

Appendix 4: 3D Printer and Calibration Software

The use of the calibration GUI can be seen in the figure below. The syringe contains water as the density of it is ~1g/ml. The allows calibration from precise extrusion volume.

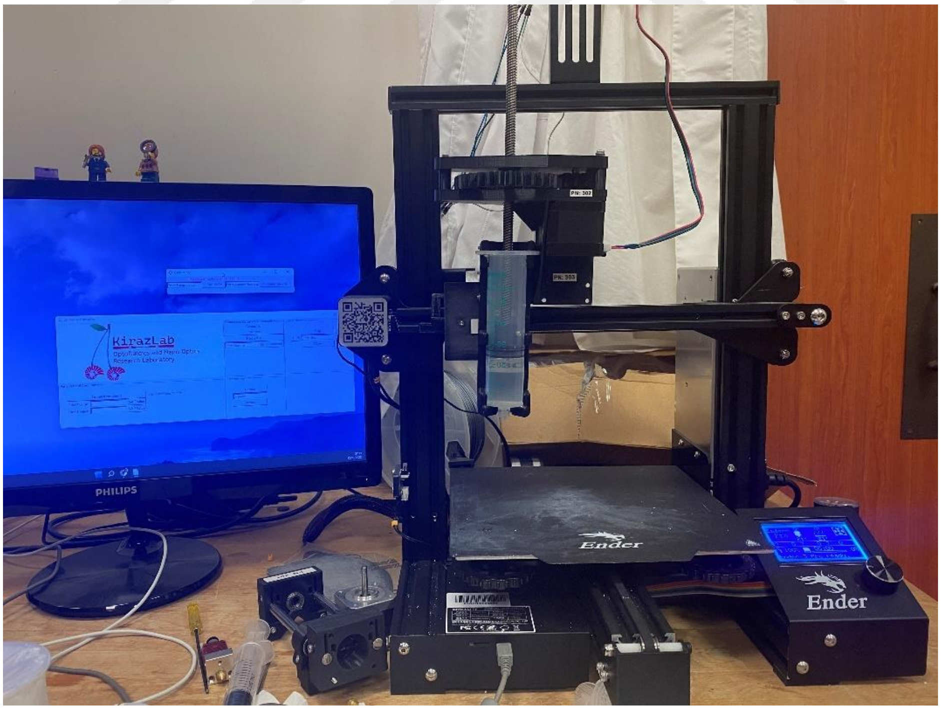

Appendix 5: Square Grid Printed Structure, Solvent Exchange.

The figure below shows a printed simple grid structure that has gone through ammonia vapor treatment. The image shows that the structure is rigid enough to handle by hand albeit delicately.

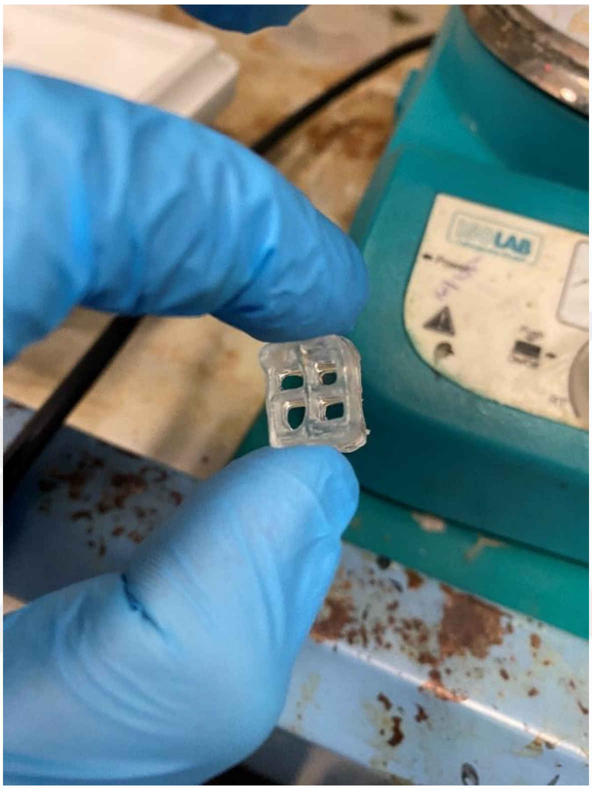

The following figure shows the solvent exchange process of the structure above.

This process takes place in a well-ventilated hood while also the beaker being sealed with parafilm and was only taken out briefly or imaging purposes.

Appendix 6: Cylindrical Structure with Inner Core During Printing

The figure below shows a TiO_2 free cylindrical structure with an inner core being printed.

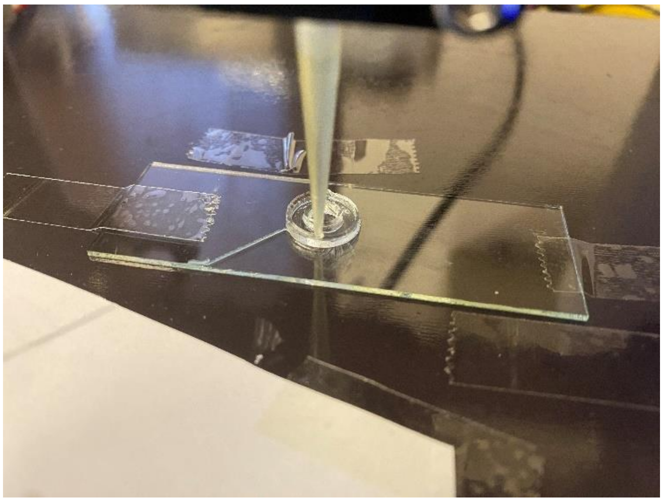

It can be seen that the inner core and outer structure do not necessarily need to be connected. The 3D printing process allows for arbitrary shaped designed and made.

Appendix 7: Dual Cylindrical Structure within Rectangle

Ink with TiO_2 printing process can be seen in the figure below.

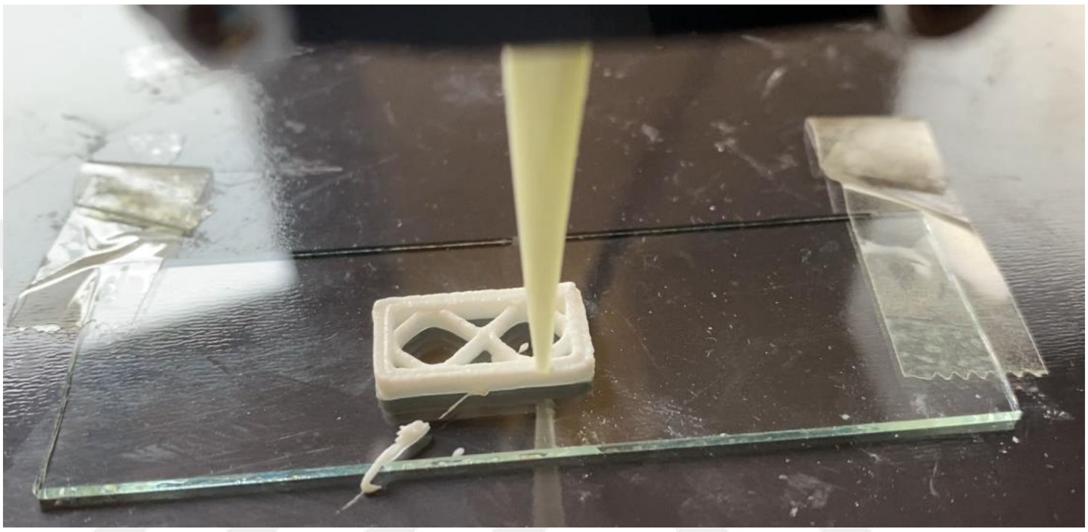

The post-process structure is shown below:

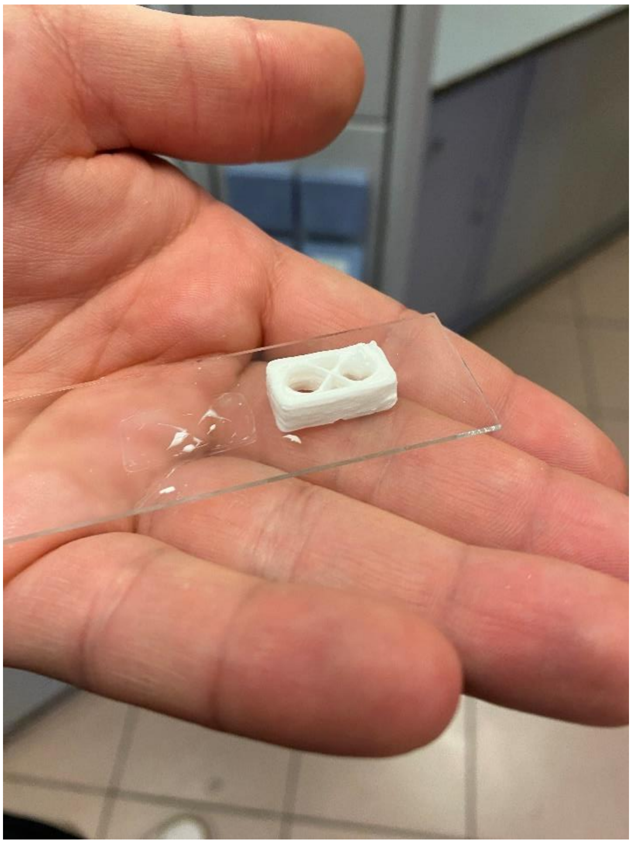

Appendix 8: Results of Air Pockets in Ink During Printing

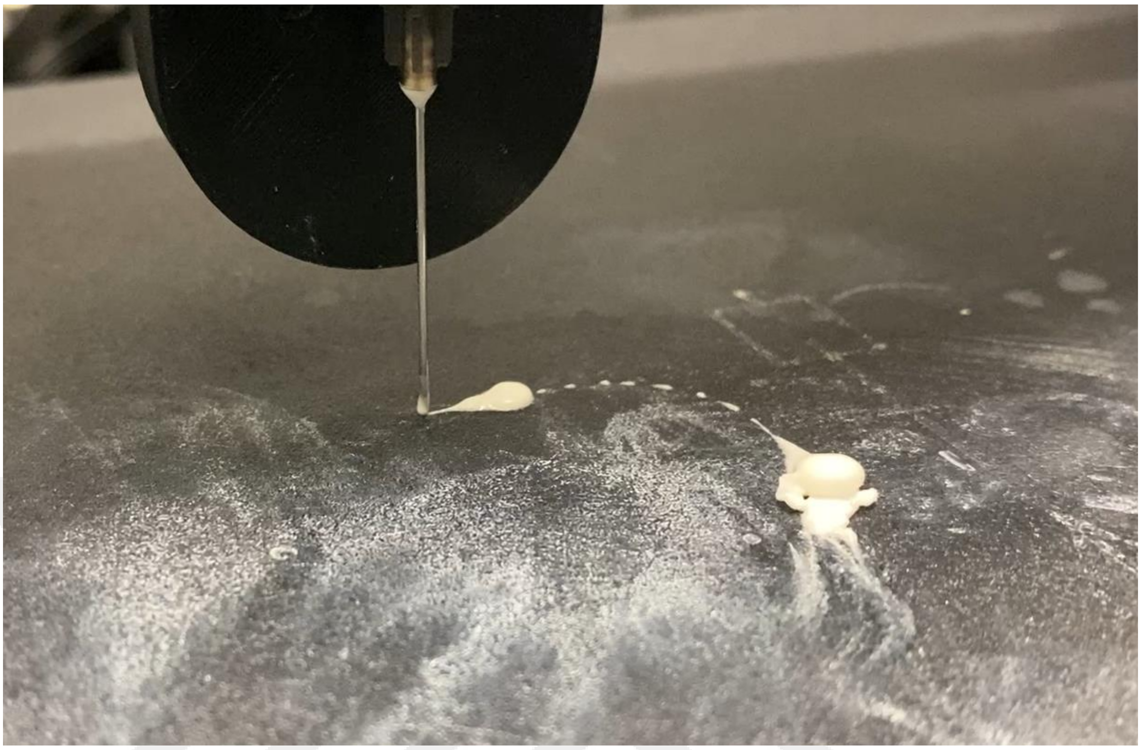

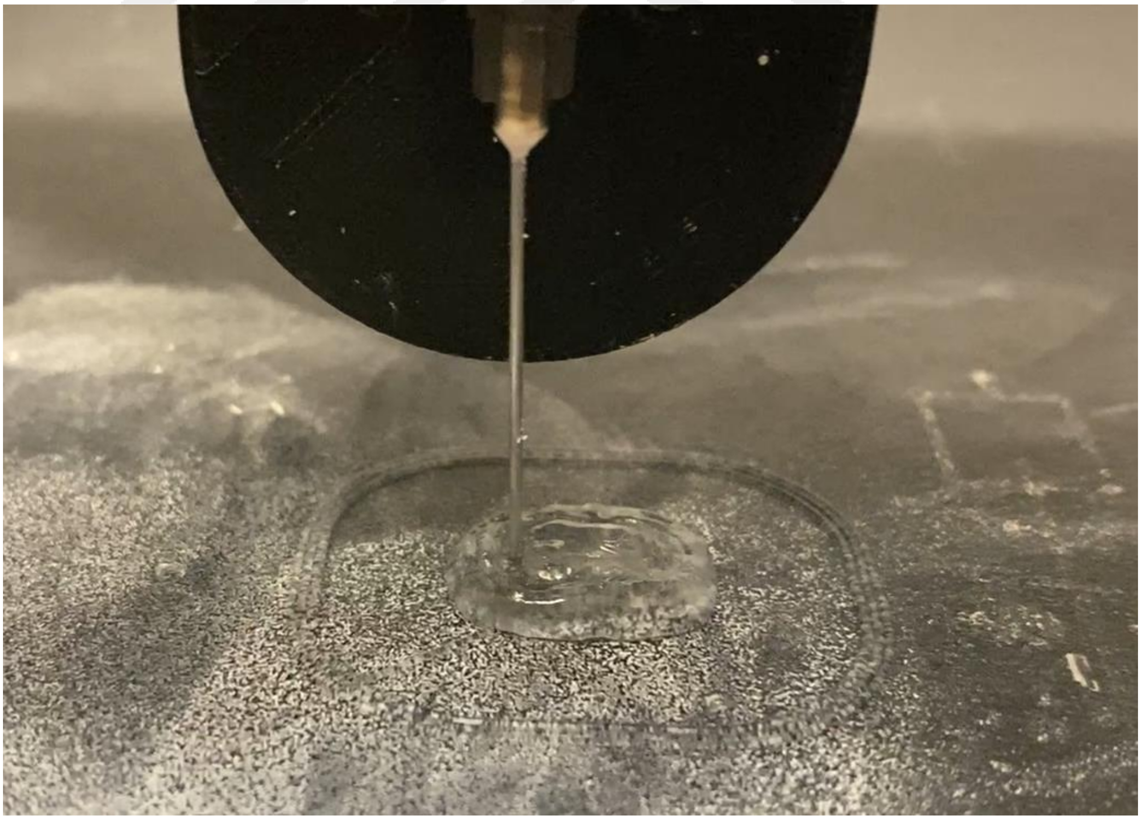

Appendix 9: Cylindrical Structure Height and Layer Lines

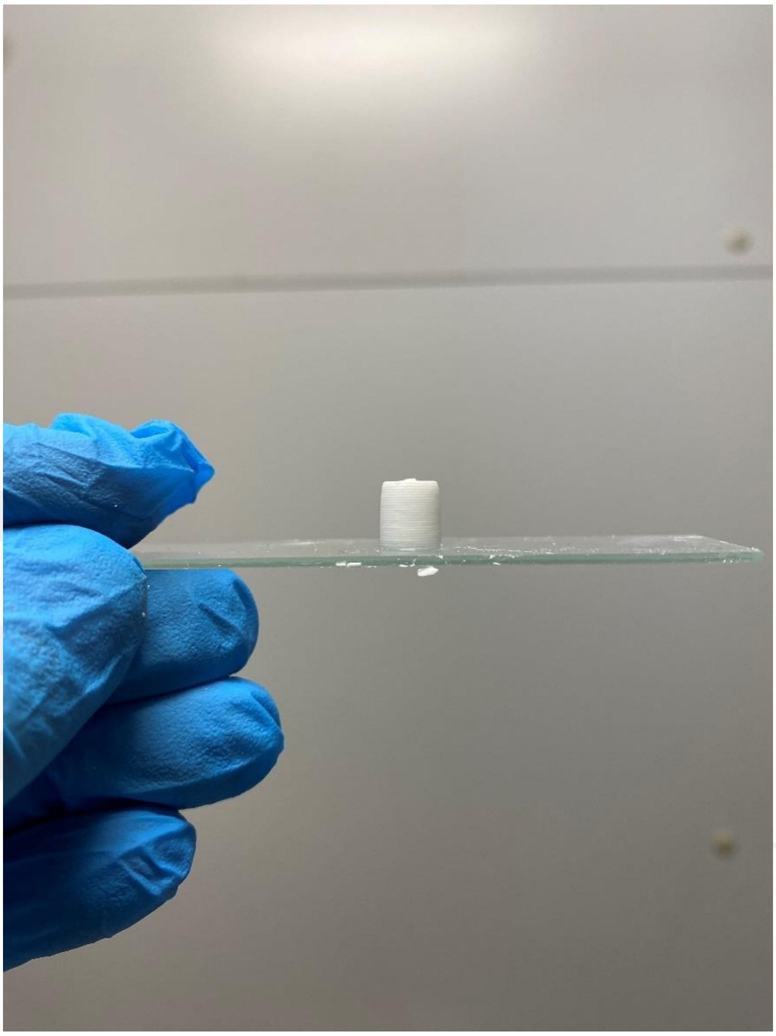

Appendix 10: Grid Patter Size

The inner distance of the calipers shown in the figure below is 10.0mm.

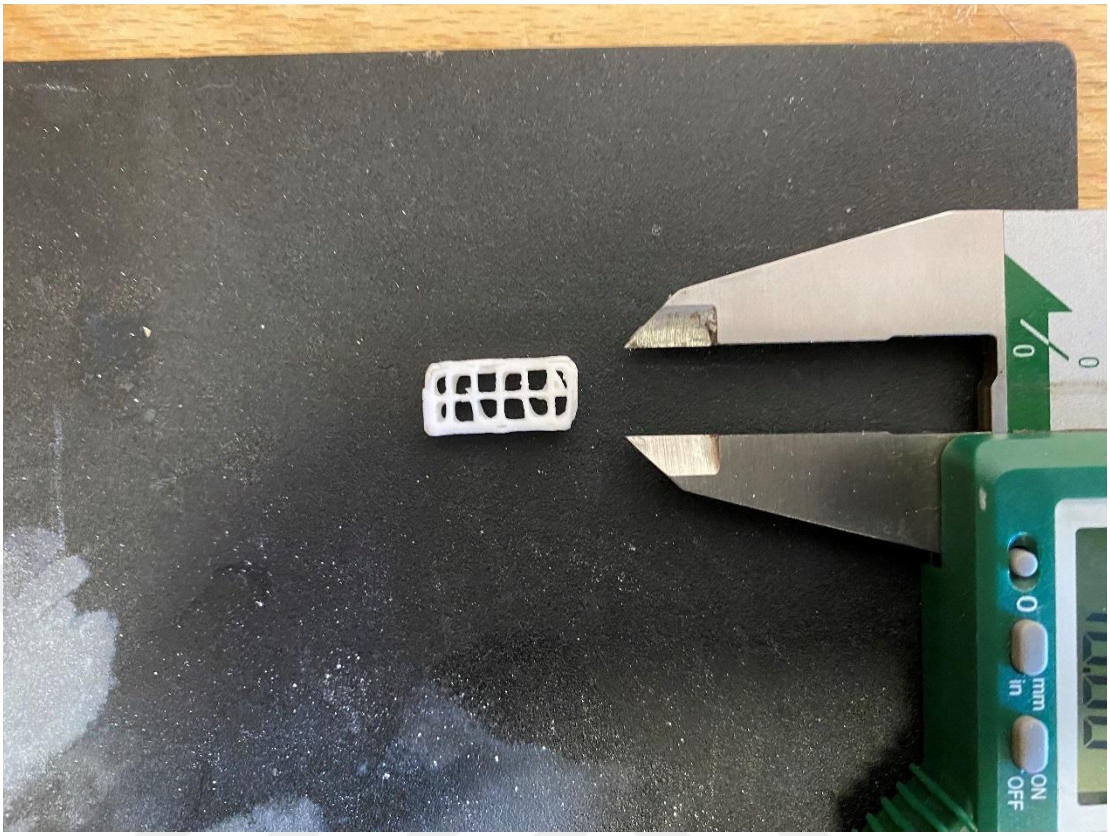
mm
in
ON
OFF

Appendix 11: Silica Aerogel Powder/Particles Added At The End Of The Ink Making Process